(2)

TECHNICAL REPORT BRL-TR-3373

BRL

SIMULATION OF BALLISTIC PHENOMENA IN CONCEPTUAL TWO-PIECE AMMUNITION

LANG-MANN CHANG
FREDERICK W. ROBBINS

JULY 1992

U.S. ARMY LABORATORY COMMAND

BALLISTIC RESEARCH LABORATORY
ABERDEEN PROVING GROUND, MARYLAND

NOTICES

REPORT DOCUMENTATION PAGE

Form Approved
OMB No. 0704-0188

1. AGENCY USE ONLY (Leave blank)	2. REPORT DATE	3. REPORT TYPE AND DATES COVERED
	July 1992	Final, Mar 91 - Dec 91

4. TITLE AND SUBTITLE

SIMULATION OF BALLISTIC PHENOMENA IN CONCEPTUAL TWO-PIECE AMMUNITION

5. FUNDING NUMBERS

PR: 1L161102AH43

6. AUTHOR(S)

Lang-Mann Chang
Frederick W. Robbins

7. PERFORMING ORGANIZATION NAME(S) AND ADDRESS(ES)

U.S. Army Ballistic Research Laboratory
ATTN: SLCBR-IB
Aberdeen Proving Ground, MD 21005-5066

8. PERFORMING ORGANIZATION REPORT NUMBER

9. SPONSORING/MONITORING AGENCY NAME(S) AND ADDRESS(ES)

U.S. Army Ballistic Research Laboratory
ATTN: SLCBR-DD-T
Aberdeen Proving Ground, MD 21005-5066

10. SPONSORING/MONITORING AGENCY REPORT NUMBER

BRL-TR-3373

11. SUPPLEMENTARY NOTES

12a. DISTRIBUTION/AVAILABILITY STATEMENT

Approved for public release; distribution unlimited.

12b. DISTRIBUTION CODE

13. ABSTRACT *(Maximum 200 words)*

Numerical simulations which examine the ballistic effects of charge configuration, location of igniter output, and interface characteristics in a conceptual two-piece cartridge are presented. The focus of this study is on the occurrence of high-amplitude pressure waves associated with these variables. Results show that all-stick charge configuration is the most forgiving system which allows a wide variety of igniter output arrangement without causing pressure wave concern. Uniform ignition along the entire charge length produces good pressure behavior in all charge configurations. Localized basepad ignition in a granular charge may result in strong pressure waves or high intergranular stress or both. The strength, impermeability, and duration of rupturing of the cartridge component interface may also strongly affect the interior ballistics. These calculated results illustrate the importance of a proper design of the charge and ignition system.

14. SUBJECT TERMS

two-piece cartridge; charge configuration; igniters; ignition; ballistic phenomena; pressure waves; intergranular stress

15. NUMBER OF PAGES 83

16. PRICE CODE

17. SECURITY CLASSIFICATION OF REPORT	18. SECURITY CLASSIFICATION OF THIS PAGE	19. SECURITY CLASSIFICATION OF ABSTRACT	20. LIMITATION OF ABSTRACT
UNCLASSIFIED	UNCLASSIFIED	UNCLASSIFIED	UL

NSN 7540-01-280-5500

Standard Form 298 (Rev. 2-89)
Prescribed by ANSI Std. Z39-18
298-102

INTENTIONALLY LEFT BLANK.

TABLE OF CONTENTS

INTENTIONALLY LEFT BLANK.

LIST OF FIGURES

INTENTIONALLY LEFT BLANK.

LIST OF TABLES

INTENTIONALLY LEFT BLANK.

ACKNOWLEDGMENTS

The authors would like to express their thanks to Mr. Albert W. Horst and Dr. Joseph J. Rocchio, both at BRL, for their encouragement to pursue this work. Special appreciation is due Ms. Tracy Keys for her assistance in providing most of the plots presented in this report and to Ms. Liz Marcou for preparing the illustrations.

INTENTIONALLY LEFT BLANK.

1. INTRODUCTION

The concept of two-piece cartridge design (see Figures 1 through 3) for the next-generation 140-mm advanced tank cannon has recently generated great interest. The two cartridge components are easier to handle than a long one-piece design and they can be separately loaded into the gun chamber. The combined length of the two cartridge components is much greater than that of conventional one-piece 105-mm or 120-mm ammunition. Particular concerns regarding the ammunition are due to its great length and the flow barrier across the cartridge case interface, which may cause uneven ignition in the two propelling charges of the cartridge. Without appropriate designs of the charges and their ignition system, the ammunition may perform poorly and, even worse, severe pressure waves may occur. In fact, the data from early firing tests with a prototype two-piece cartridge consisting of two stick propelling charges ignited by a single basepad at the breech end showed high-amplitude pressure waves. Such pressure waves have been implicated in the catastrophic overpressure of several artillery and tank cannons (May and Horst 1978; Horst 1986). To help eliminate the potential hazard, a guideline for the development of the ammunition is necessary.

The present work is performed to examine ballistic phenomena in response to variations of charge configuration, location of igniter output, and an internal flow barrier, as shown in Figures 1 through 3. These three areas are major factors determining the performance of the propulsion system of the two-piece cartridge. In the case that both cartridge components are packed with granular propellant, Chang (1990) has examined the ballistic effects from the flow barrier at the interface as well as from igniter output distribution. In this study, we attempt to include all of the four possible combinations of granular and stick charges. As to the igniter output distribution, it is extended to include local ignition by a basepad (which is most likely to cause high-amplitude pressure waves). Furthermore, a broader description of interface characteristics is considered. The focus of this study is on the occurrence of high-amplitude pressure waves associated with these variables.

The computer code employed for calculations is the two-phase flow code XKTC (Gough 1986). Of the features of the code which are important in the present application is its capability of accounting for:

- o intrusion of projectile afterbody
- o cross-sectional area change along the gun chamber
- o igniter output as a function of time and location
- o combustion of the cartridge case and cartridge case interface
- o strength and permeability of the cartridge case interface

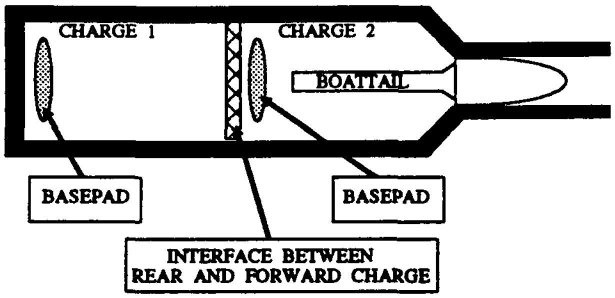

Figure 1. <u>Base Ignition; [bn|bn]</u>

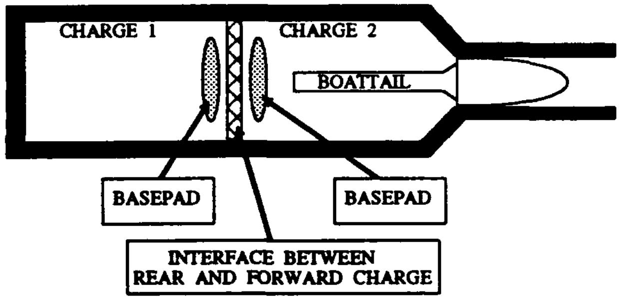

Figure 2. <u>Center Ignition; [nb|bn]</u>

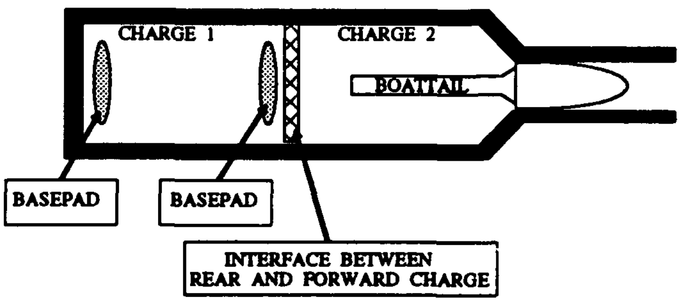

Figure 3. <u>Ignition at Both Ends of the Rear Charge; [bb|nn]</u>

2. MODELING

2.1 Data Used. The following data are generic and are common for all calculations.

Propellants - cylindrical granular JA2 and partially-cut stick JA2. Both have 19 perforations, perforation diameter = 0.074 cm, grain length = 1.9 cm, grain diameter = 0.83 cm, mass in the rear cartridge component = 7.25 kg, and mass in the forward cartridge component = 8.16 kg.

Projectile mass = 13.6 kg.

Igniter material in the basepad - black powder, 91 grams.

Gun dimensions - indicated in Figure 4.

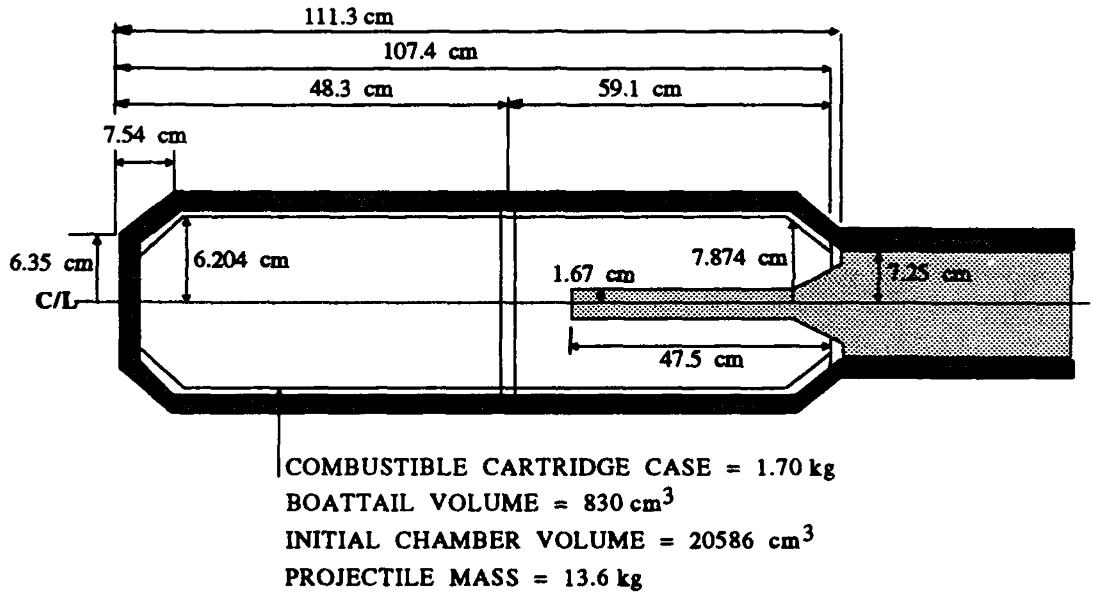

Figure 4. Chamber Dimensions

2.2 Charge Configurations. There are four different combinations of granular and stick propellant beds in the two-piece cartridge. For simplicity of reference, we use the following symbols to represent them (note: g = granular and s = stick):

(s,s) - stick propellant in both the rear and the forward cartridge components.

(s,g) - stick propellant in the rear cartridge component and granular propellant in the forward cartridge component.

{g,s} - granular propellant in the rear cartridge component and stick propellant in the forward cartridge component.

{g,g} - granular propellant in both the rear and the forward cartridge components.

2.3 Locations of Igniter Output. It has been recognized that the location of igniter output has a profound effect on ballistic behavior. Without being directed to a specific case, we consider two general categories of igniter output distribution. One is uniform ignition along the charge length and the other is local ignition from basepad igniters placed at the end regions of the two charges in the cartridge, see Figures 1 through 3. Uniform ignition here is defined as simultaneous ignition everywhere in the charge. It can be achieved by a scheme such as multi-point ignition through the use of laser pulses or electric igniters. As to local ignition, three arrangements are considered. The first arrangement is that a basepad is placed at the rear end (breech end) of the rear charge and another basepad at the rear end of the forward charge, as shown in Figure 1. The second arrangement is called center ignition in which two basepads are placed against the two faces of the cartridge case interface, as shown in Figure 2. The last arrangement is that two basepads are placed in the rear charge, one at each end, as shown in Figure 3.

We also consider that the igniter in one of the two cartridge components may fail to function, leaving that cartridge component to be ignited by the combustion products of the other cartridge component. We then choose nine cases to study, as listed in Table 1. Again, for simplicity, symbols are used to represent those cases. In the table, "u" = uniform ignition, "b" = basepad location, "n" = no ignition source, and "|" = interface. As an example, Figure 3 would be [bb|nn], i.e., basepad ignition occurring at the rear and forward ends of the rear component of the cartridge.

2.4 Cartridge Cases and Cartridge Case Interface. Both the cartridge cases and their interface are considered as energetic material. The cartridge case interface is modeled as an end wall of one of the two cartridge components. The mass of the end wall is 0.12 kg and it is consumed totally in 3 ms after the surface temperature of adjacent propellant grains reach an assumed ignition temperature (171°C).

The flow barrier at the cartridge case interface is characterized by:

- o The shear strength of the interface.
- o The permeability of the interface.
- o The duration from the start to the completion of rupture of the interface.

Table 1. Locations of Igniter Output

	uniform ignition		local ignition (basepad ignition)		
	rear charge	fwd charge	rear charge		fwd charge
Symbol			rear end	fwd end	rear end
[uu|uu]	x	x	-	-	-
[uu|nn]	x	-	-	-	-
[nn|uu]	-	x	-	-	-
[bn|bn]	-	-	x	-	x
[bn|nn]	-	-	x	-	-
[nn|bn]	-	-	-	-	x
[nb|bn]	-	-	-	x	x
[nb|nn]	-	-	-	x	-
[bb|nn]	-	-	x	x	-

where

[uu|uu] - simultaneous ignition occurring everywhere in both the rear and the forward charges.

[uu|nn] - simultaneous ignition occurring everywhere in the rear charge, but no igniter output in the forward charge.

[nn|uu] - simultaneous ignition occurring everywhere in the forward charge, but no igniter output in the rear charge.

[bn|bn] - basepad ignition occurring at the breech end of the rear charge and at the rear end of the forward charge.

[bn|nn] - basepad ignition occurring at the breech end of the rear charge.

[nn|bn] - basepad ignition occurring at the rear end of the forward charge.

[nb|bn] - basepad ignition occurring at the forward end of the rear charge and at the rear end of the forward charge; i.e., on both sides of the cartridge interface.

[nb|nn] - basepad ignition occurring at the forward end of the rear charge.

[bb|nn] - basepad ignition occurring at the rear and the forward ends of the rear charge.

We classify the shear strength of the interface as either "strong" or "weak". Here "strong" and "weak" mean that the interface starts rupturing when the pressure difference between the two faces of the interface reaches 7 MPa (1000 psi) and 3.5 MPa (500 psi), respectively. These pressure values are determined as follows:

$$p = [3.14 \times D \times t]S \; / \; [0.25 \times 3.14 \times D^2]$$

where p = pressure difference between the two faces of the interface.

D = inside diameter of the cartridge case, 150.5 mm.

t = thickness of the interface, 6.35 mm.

S = shear strength of the interface.

From the manufacturer (Armtec, CA), the shear strength ranges from 21 MPa (3000 psi) to 42 MPa (6000 psi) depending upon the density of the interface. Substituting these two strength values into the formula, the two pressure differences specified above are obtained. It is noted that the interface has been assumed to have little support from the propellant bed on the low pressure side.

The permeability of the interface is also taken into account since in some cases the interface may be perforated in order to reduce the effect of the flow barrier to flamespreading. Two values are assumed for the permeability: totally impermeable (i.e., permeability is 0%) and semi-permeable (i.e., permeability is 50%).

Finally, the duration for the interface to completely rupture is another key characteristic needed to be defined in calculations. Although no measured value is available, 0.5 ms seems to be a reasonable value, with which a good match has been obtained between the calculated pressure profiles and the test data which will be given below.

3. RESULTS AND DISCUSSIONS

3.1 Matching Case. Prior to performing calculations for the charge design concepts described above, calculations for a test case to match available firing data were carried out. This practice not only validates the capability of the computer code employed, but also determines some of the input data which are not available for the code. These input data include the gun bore resistance to projectile motion and the duration of the rupturing of the cartridge case interface.

The available test data are from the firings of a 145-mm ballistic measurement facility at the U.S. Army Ballistic Research Laboratory with a two-piece cartridge packed with granular JA2 propellant in its two components. The ignition system used in the cartridge was a long metal tube primer which intruded substantially into the forward cartridge component. The output rate, a function of location and time, of the primer was determined from open air tests conducted previously during the development of two-piece cartridges for the 140-mm advanced tank cannon system (Chang, Deas, and Grosh 1991).

Figure 5 presents pressure data at the breech end and at the forward end of the gun chamber recorded from the test firing (dashed lines) of a 145-mm gun and from XKTC calculations (solid lines). In the figure, the curve dP is the result of the breech pressure minus the forward chamber pressure. The agreement between the test data and the calculations is reasonably good.

3.2 Calculated Results. Appendix A presents a typical input data file for the calculations. As mentioned earlier, there are 4 charge configurations to be examined and each of them has 9 different locations of igniter output (see Table 1). In addition, in each of these cases there are 5 different interface characteristics (strong, weak, impermeable, semi-permeable, and no interface). Apparently, a very large matrix of calculated results is obtained, as seen in Table 2. The results in Table 2 include the maximum chamber pressure (P_{max}) which occurs at the breech end, the maximum negative pressure differential (-dP) between the breech end and the forward end of the gun chamber, and the maximum intergranular stress ($S_{i,max}$) in the propellant bed.

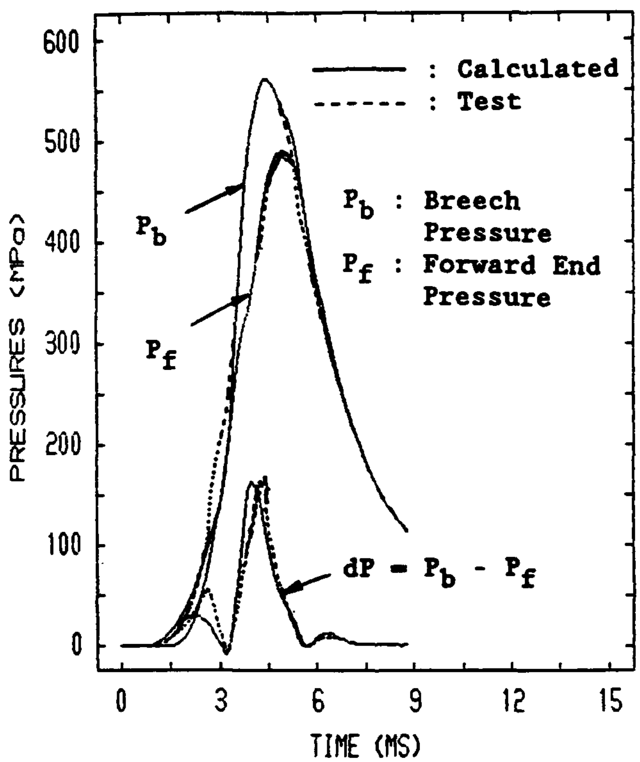

Figure 5. Calculated Result and Test Data in Matching Case

The intergranular stress refers to the average intrinsic stress which the propellant bed would experience at each cross-sectional plane due to the load carried by the solid phase alone. The stress occurs when the propellant bed is under compaction as a result of a non-uniform pressure distribution along the propellant bed. The stress can be a function of time and location along the gun chamber length. Normally, the stress reaches its maximum value immediately before the projectile starts to move. When the stress increases, the grain may deform or even fracture; depending on the propellant formulation, temperature, and rate of compression on the grain. M30 and LOVA propellants may fracture without much deformation. JA2 propellant may deform to a very large degree without fracture at temperatures above $0^{o}C$. However, when conditioned to -20°C or below, JA2 may easily fracture when the stress exceeds a certain limit (Lieb 1991). Upon fracture, the burning surface area of the propellant grain increases. This may lead to a locally enhanced mass generation rate in the propellant bed, which may drive high-amplitude pressure waves. The present calculations do not account for the effect of grain fracture on the ballistic performance.

Appendixes B through E present the pressure-time traces at the breech and the forward end of the chamber, and their differential for all of the charge configurations listed in Table 2.

Based on the results given in Table 2, Table 3 is established to summarize the physical phenomena occurring in each of the four charge configurations with igniters located at specified locations. In the table, note that for pressure waves: "small" means < 7 MPa, "moderate" means > 7 MPa but < 35 MPa, "strong" means > 35 MPa but < 70 MPa, "very strong" means > 70 Mpa. This classification is established based on the experience obtained from firing tests with 105-mm and 120-mm tank gun systems. As to the maximum intergranular stress ($S_{i,max}$); "low" means < 3.5 MPa, "moderate" means > 3.5 MPa but < 7 MPa, "high" means > 7 MPa but < 15 MPa, and "very high" means > 15 MPa. It is noted that this classification is established based on limited test data gathered from the testing using a controlled test fixture (Lieb 1991). In spite of this, it is felt that the classification is reasonable in consideration of the fact that JA2 grains may fracture at temperatures below -20°C.

In Table 3, there is a great deal of interesting information to be discussed. Without attempting to cover all of the information, we present only those of primary concern regarding the formation of high-amplitude pressure waves which may cause safety hazards.

3.2.1 Effects of Charge Configuration. With a focus on the charge configuration, the following summary is made in reference to Tables 2 and 3.

o Configuration (s,s) -- has no pressure waves problem from uniform ignition [uu|uu] or basepad ignition at the rear ends of both charges [bn|bn] or center ignition [nb|bn].

Table 2. Calculated Results

Symbols: imp = impermeable; per = semi-permeable.

Charge	Igniter	Interface strength	Interface permeability	P_{max} (MPa)	$-dP$ (MPa)	$S_{1\,max}$ (MPa)
	[uu|uu]	no interface		560	0	0
		strong	imp	559	0	0
		strong	per	591	0	0
		weak	imp	567	0	0
		weak	per	574	0	0
(s,s)	[uu|nn]	no interface		557	4	2
		strong	imp	555	30	10
		strong	per	556	33	9
		weak	imp	572	18	9
		weak	per	576	18	5
	[nn|uu]	no interface		558	3	2
		strong	imp	559	16	23
		strong	per	561	21	42
		weak	imp	559	16	23
		weak	per	559	14	25
	[bn|bn]	no interface		578	6	2
		strong	imp	585	1	5
		strong	per	604	1	3
		weak	imp	583	1	5
		weak	per	592	1	3
(s,s)	[bn|nn]	no interface		560	8	2
		strong	imp	566	31	10
		strong	per	579	29	6
		weak	imp	570	28	10
		weak	per	579	24	6
	[nn|bn]	no interface		564	1	1
		strong	imp	572	25	49
		strong	per	571	23	31
		weak	imp	574	18	29
		weak	per	571	16	18
(s,s)	[nb|bn]	no interface		565	1	3
		strong	imp	572	0	3
		strong	per	594	1	3
		weak	imp	584	4	4
		weak	per	594	4	4
	[nb|nn]	no interface		566	1	2
		strong	imp	554	35	32
		strong	per	555	34	20
		weak	imp	566	21	19
		weak	per	574	18	19
(s,s)	[bb|nn]	no interface		579	9	4
		strong	imp	570	36	8
		strong	per	572	34	7
		weak	imp	581	19	8
		weak	per	591	14	7

Table 2. Calculated Results (Cont'd)

Charge	Igniter	Interface strength	Interface permeability	P_{max} (MPa)	-dP (MPa)	$S_{i\,max}$ (MPa)
	[uu|uu]	no interface		565	0	0
		strong	imp	552	0	1
		strong	per	566	0	1
		weak	imp	554	0	1
		weak	per	553	0	1
{s,g}	[uu|nn]	no interface		532	15	3
		strong	imp	599	108	11
		strong	per	603	108	6
		weak	imp	572	81	7
		weak	per	571	80	6
	[nn|uu]	no interface		593	8	6
		strong	imp	565	14	44
		strong	per	572	13	35
		weak	imp	557	8	27
		weak	per	557	7	20
	[bn|bn]	no interface		539	15	3
		strong	imp	577	19	45
		strong	per	570	14	40
		weak	imp	566	6	20
		weak	per	562	6	31
{s,g}	[bn|nn]	no interface		533	41	1
		strong	imp	599	95	1
		strong	per	601	95	2
		weak	imp	591	87	2
		weak	per	581	83	2
	[nn|bn]	no interface		540	12	1
		strong	imp	552	8	14
		strong	per	548	10	32
		weak	imp	546	12	31
		weak	per	545	14	19
	[nb|bn]	no interface		556	13	1
		strong	imp	579	17	26
		strong	per	571	4	14
		weak	imp	561	6	8
		weak	per	559	4	14
{s,g}	[nb|nn]	no interface		554	13	1
		strong	imp	637	174	19
		strong	per	570	85	3
		weak	imp	609	133	11
		weak	per	568	82	3
{s,g}	[bb|nn]	no interface		545	23	5
		strong	imp	636	125	16
		strong	per	634	125	10
		weak	imp	620	102	11
		·eak	per	615	93	10

Table 2. Calculated Results (Cont'd)

Charge	Igniter	Interface strength	Interface permeability	P_{max} (MPa)	-dP (MPa)	$S_{i\,max}$ (MPa)
	[uu|uu]	no interface		550	1	0
		strong	imp	582	1	1
		strong	per	611	4	0
		weak	imp	588	2	0
		weak	per	583	2	0
{g,s}	[uu|nn]	no interface		539	3	2
		strong	imp	557	31	0
		strong	per	551	28	0
		weak	imp	564	20	0
		weak	per	580	17	0
	[nn|uu]	no interface		557	10	22
		strong	imp	665	107	31
		strong	per	685	131	13
		weak	imp	637	82	21
		weak	per	629	62	13
	[bn|bn]	no interface		544	32	9
		strong	imp	640	16	14
		strong	per	663	10	8
		weak	imp	616	10	9
		weak	per	617	9	8
{g,s}	[bn|nn]	no interface		579	3	7
		strong	imp	539	46	11
		strong	per	540	45	11
		weak	imp	530	42	11
		weak	per	487	38	19
	[nn|bn]	no interface		579	3	7
		strong	imp	679	137	25
		strong	per	699	133	20
		weak	imp	648	61	18
		weak	per	651	41	14
	[nb|bn]	no interface		595	4	8
		strong	imp	604	3	12
		strong	per	629	6	11
		weak	imp	609	5	8
		weak	per	616	6	11
{g,s}	[nb|nn]	no interface		579	3	7
		strong	imp	570	0	34
		strong	per	578	0	23
		weak	imp	574	0	19
		weak	per	586	0	17
{g,s}	[bb|nn]	no interface		544	32	9
		strong	imp	593	0	8
		strong	per	599	0	3
		weak	imp	590	0	4
		weak	per	591	0	3

Table 2. Calculated Results (Cont'd)

Charge	Igniter	Interface strength	Interface permeability	P_{max} (MPa)	-dP (MPa)	$S_{i\,max}$ (MPa)
(g,g)	[uu|uu]	no interface		565	0	0
		strong	imp	579	0	1
		strong	per	581	0	1
		weak	imp	566	0	1
		weak	per	578	0	1
	[uu|nn]	no interface		522	21	4
		strong	imp	608	90	10
		strong	per	602	76	4
		weak	imp	579	63	6
		weak	per	574	57	10
	[nn|uu]	no interface		605	12	8
		strong	imp	693	131	26
		strong	per	729	144	15
		weak	imp	663	79	17
		weak	per	654	62	15
(g,g)	[bn|bn]	no interface		548	39	5
		strong	imp	594	5	15
		strong	per	616	0	8
		weak	imp	591	0	8
		weak	per	578	0	8
	[bn|nn]	no interface		569	72	8
		strong	imp	647	117	10
		strong	per	646	115	12
		weak	imp	634	105	8
		weak	per	631	102	8
	[nn|bn]	no interface		549	0	9
		strong	imp	628	22	24
		strong	per	659	35	20
		weak	imp	600	6	16
		weak	per	593	3	15
(g,g)	[nb|bn]	no interface		563	0	8
		strong	imp	591	16	11
		strong	per	621	19	11
		weak	imp	581	2	11
		weak	per	594	0	11
	[nb|nn]	no interface		549	0	9
		strong	imp	693	191	26
		strong	per	593	91	12
		weak	imp	560	39	9
		weak	per	554	26	12
(g,g)	[bb|nn]	no interface		548	39	5
		strong	imp	589	53	7
		strong	per	590	52	6
		weak	imp	572	28	4
		weak	per	572	26	6

Table 3. Physical Phenomena

Pressure Waves:
small = < 7 MPa
moderate = > 7 MPa but < 35 MPa
strong = > 35 MPa but < 70 MPa
very strong = > 70 MPa

Maximum Intergranular Stress:
low = < 3.5 MPa
moderate = > 3.5 MPa but < 7 MPa
high = > 7 MPa but < 15 MPa
very high = > 15 MPa

Granulation: Stick Propellant in Both the Rear and the Forward Charges, (s,s)

Igniter	Pressure Waves	Interface Effect	Max. Inter. Stress
[uu|uu]	none	no noticeable effect	none
[uu|nn]	moderate, increasing with interface strength	strong effect from strength, small effect from impermeability	moderate to high, increasing with interface strength and impermeability
[nn|uu]	moderate	moderate effect from strength, small effect from impermeability	very high
[bn|bn]	very small	no significant effect	moderate
[bn|nn]	moderate, increasing with interface strength	strong effect from strength, small effect from impermeability	moderate to high, increasing with interface impermeability
[nn|bn]	moderate, increasing with interface strength	moderate effect from strength, small effect from impermeability	very high increasing with interface strength and impermeability
[nb|bn]	small	no significant effect	low
[nb|nn]	moderate to strong, increasing with interface strength	strong effect from strength, small effect from impermeability	very high increasing with interface strength
[bb|nn]	moderate to strong, increasing with interface strength	strong effect from strength, small effect from impermeability	high

Table 3. Physical Phenomena (Cont'd)

Granulation: Stick in the Rear Charge and Granular in the Forward Charge. {s,g}

Igniter	Pressure Waves	Interface Effect	Max. Inter. Stress
[uu|uu]	none	no noticeable effect	very small
[uu|nn]	very strong	strong effect from strength	moderate to high, increasing with interface strength and impermeability
[nn|uu]	moderate	moderate effect from strength, small effect from impermeability	very high increasing with interface strength and impermeability
[bn|bn]	moderate	moderate effect from strength, small effect from impermeability	very high increasing with interface strength
[bn|nn]	very strong	strong effect from strength, small effect from impermeability	low
[nn|bn]	moderate, tends to reduce with interface added	small effect from strength	very high
[nb|bn]	small to moderate	small effect from both strength and impermeability	high
[nb|nn]	very strong	strong effect from both strength and impermeability	low to high, increasing with strength and impermeability
[bb|nn]	very strong	strong effect from strength	high, increasing with strength and impermeability

Table 3. Physical Phenomena (Cont'd)

Granulation: Granular in the Rear Charge and Stick in the Forward Charge. (g,s)

Igniter	Pressure Waves	Interface Effect	Max. Inter. Stress
[uu|uu]	small	no significant effect	none
[uu|nn]	moderate	moderate effect from strength	none
[nn|uu]	very strong	strong effect from strength	high to very high, increasing with interface strength and impermeability
[bn|bn]	moderate, reduced with interface added	moderate effect from both strength and impermeability	high
[bn|nn]	strong	moderate effect from strength, small effect from impermeability	high
[nn|bn]	very strong	very strong effect from strength, moderate effect from impermeability	very high increasing with interface strength and impermeability
[nb|bn]	small	small effect from both strength and impermeability	high
[nb|nn]	none	no noticeable effect from strength and impermeability	very high increasing with interface strength
[bb|nn]	reduced to none with interface added		moderate

Table 3. Physical Phenomena (Cont'd)

Granulation: Granular Propellant in Both the Rear and the Forward Charges, {g,g}

Igniter	Pressure Waves	Interface Effect	Max. Inter. Stress
[uu|uu]	none	no effect	very low
[uu|nn]	very strong	strong effect from both strength and impermeability	moderate to high
[nn|uu]	very strong	strong effect from strength	very high
[bn|bn]	reduced to small or none with interface added		high
[bn|nn]	very strong	strong effect from strength	high increasing with interface strength
[nn|bn]	moderate	moderate effect from strength and impermeability	very high
[nb|bn]	moderate	moderate effect from strength	high
[nb|nn]	very strong	very strong effect from both strength and permeability	high
[bb|nn]	strong	strong effect from strength	moderate

o Configuration {s,g} -- has no pressure waves problem from uniform ignition [uu|uu] only. It is interesting to note that from [bn|bn] and [nn|bn] ignition the pressure waves tend to reduce from moderate to small when the interface is inserted. However, in consideration of the resultant high intergranular stress (which may cause grain fracture) occurring in the forward charge (granular), the actual wave amplitude may increase significantly.

o Configuration {g,s} -- has no pressure waves problem from uniform ignition [uu|uu] only. Although [nb|nn] ignition produces no pressure waves, the resultant high intergranular stress occurring in the rear charge may cause high-amplitude pressure waves.

o Configuration {g,g} -- has no pressure waves problem from uniform ignition [uu|uu] only. The result also shows that from [bn|bn] ignition the pressure waves are reduced from strong to small or to none when the interface is inserted. However, there is a noticeable increase in the intergranular stress in both charges, which may cause grain fracture and thus high-amplitude pressure waves.

3.2.2 Effects of Location of Igniter Output. When the igniter location is considered, we may also establish the following summary based on the data given in Tables 2 and 3.

o Uniform Ignition [uu|uu] -- produces good pressure behavior with no pressure waves for all charge configurations, as exhibited in Figure 6.

o Center Ignition [nb|bn] -- produces good pressure behavior with no or very low pressure waves in the charge configurations {s,s} and {g,s}. The ignition produces moderate pressure waves in the other two charge configurations and a moderately high intergranular stress, see Figure 7 and Table 2.

o Base Ignition in Both Charges [bn|bn] -- produces good pressure behavior with no pressure waves in the charge configuration {s,s}. The ignition produces moderate pressure waves and a very high intergranular stress in the charge configuration {s,g}. In the charge configuration {g,s}, the ignition produces moderate pressure waves and a moderately high intergranular stress. It is surprising that in the charge configuration {g,g}, pressure waves are reduced from high to almost none after an interface is inserted; however, the intergranular stress is moderately high, see Figure 8 and Table 2.

o Basepad ignition at the breech end of the cartridge [bn|nn] -- produces strong pressure waves in all charge configurations with the exception of the charge configuration {s,s} in which the pressure waves are moderate, see Figure 9.

o A granular charge with ignition at one end: [bn|nn], [bn|bn], [nb|nn], [nb|bn], [nn|bn], -- produces a high intergranular stress, but not necessarily high-amplitude pressure waves; see Figure 10.

o A granular charge ignited by its adjacent charge: [uu|nn], [bn|nn], [nb|nn], [bb|nn], [nn|uu], nn|bn] -- produces strong pressure waves in all charge configurations (see Figure 11 for example) with the exception of the charge configuration (g,g) with [nn|bn] ignition, which produces moderate pressure waves. The resultant intergranular stress is also high in most cases.

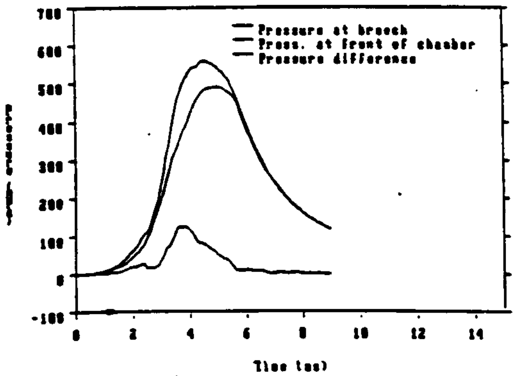

(s,s)/[uu|uu]/st imp

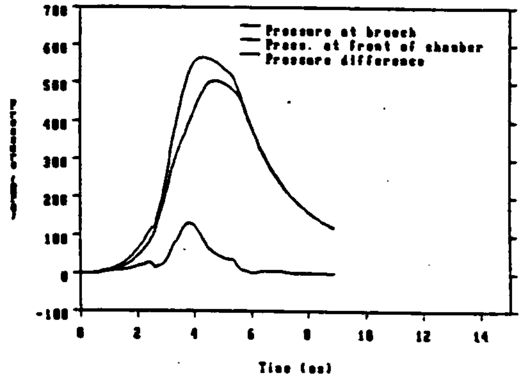

(s,g)/[uu|uu]/st imp

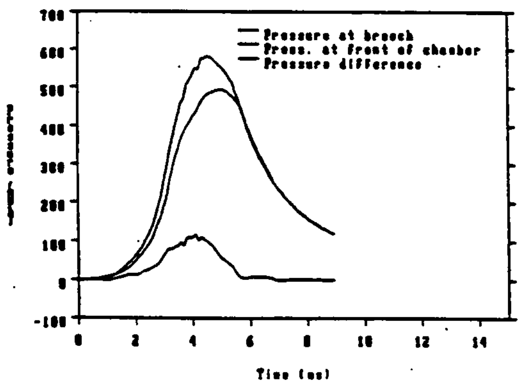

(g,s)/[uu|uu]/st imp

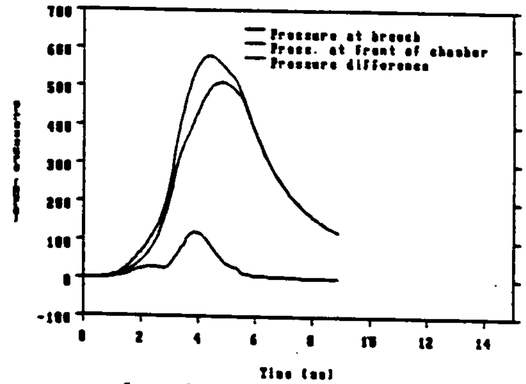

(g,g)/[uu|uu]/st imp

where: st imp = strong impermeable interface

Figure 6. Pressure Data for Uniform Ignition, [uu|uu]

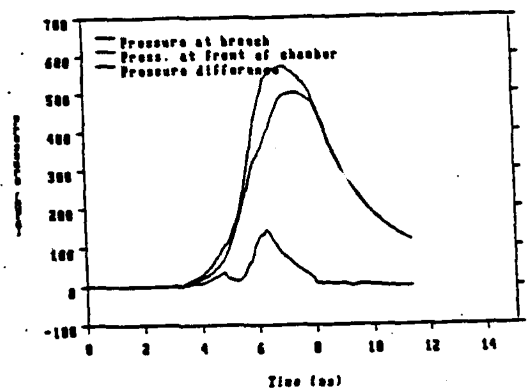

(s,s)/[nb|bn]/st imp

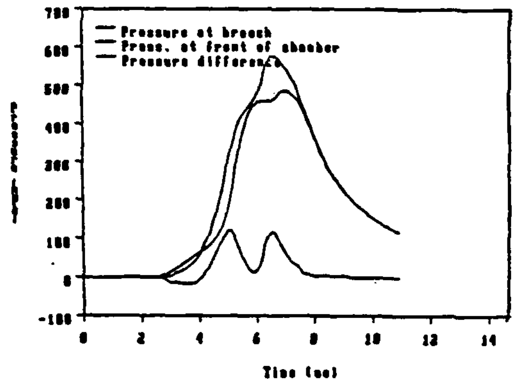

(s,g)/[nb|bn]/st imp

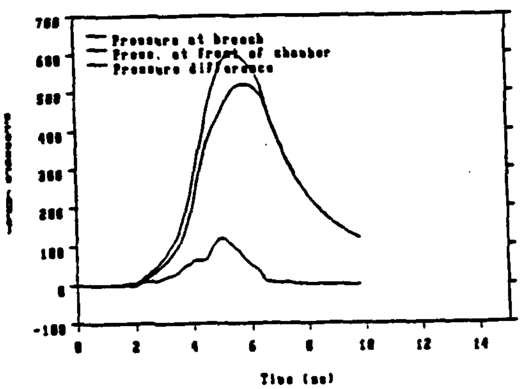

(g,s)/[nb|bn]/st imp

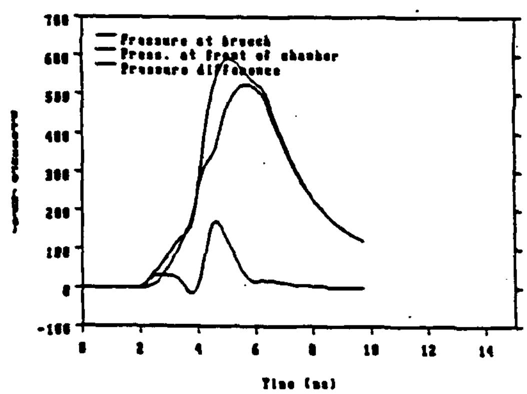

(g,g)/[nb|bn]/st imp

Figure 7. Pressure Data for Center Ignition, [nb|bn]

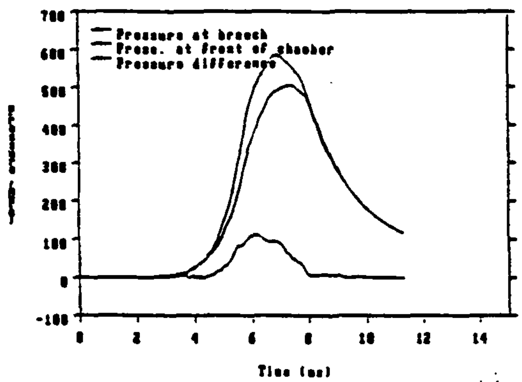

(s,s)/[bn|bn]/st imp

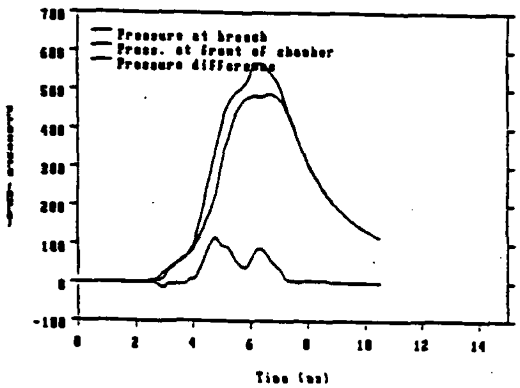

(s,g)/[bn|bn]/st per

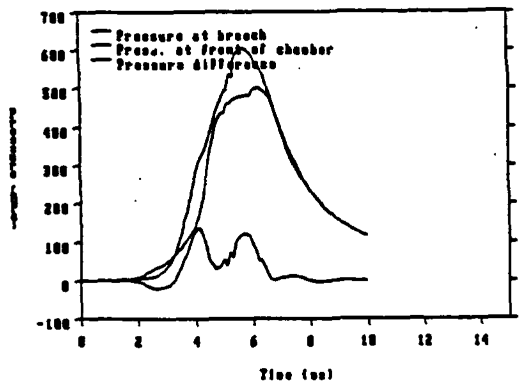

(g,s)/[bn|bn]/st imp

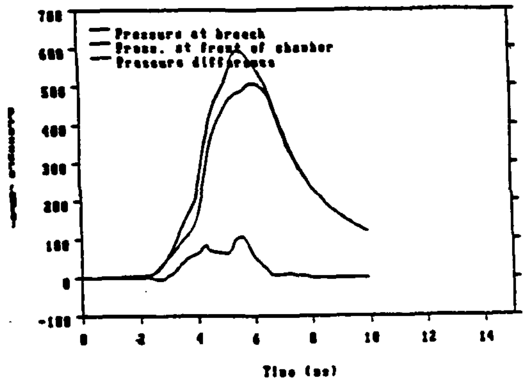

(g,g)/[bn|bn]/st imp

Figure 8. Pressure Data for Base Ignition. [bn|bn]

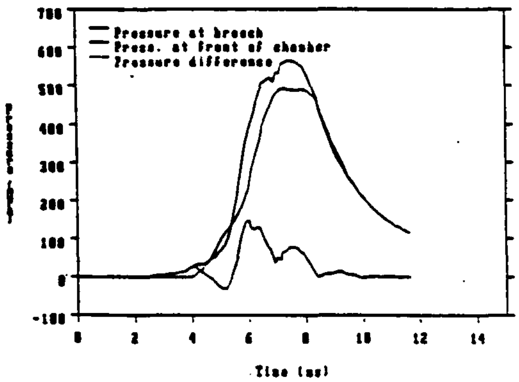

{s,s}/[bn|nn]/st imp

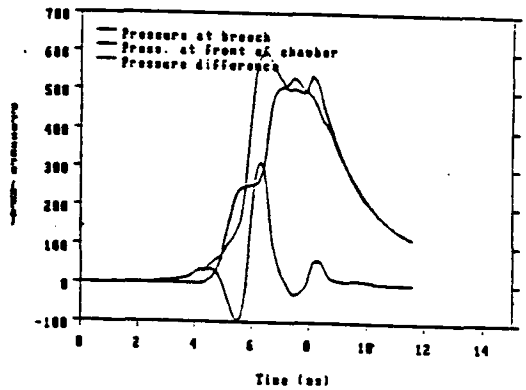

{s,g}/[bn|nn]/st imp

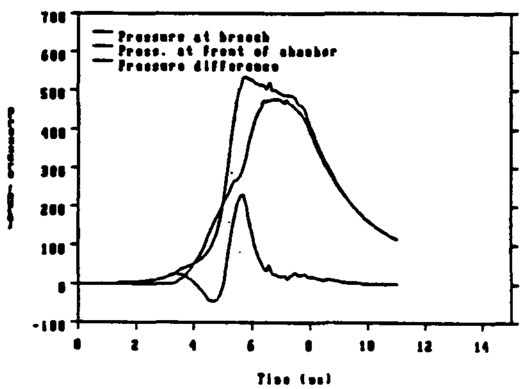

{g,s}/[bn|nn]/st imp

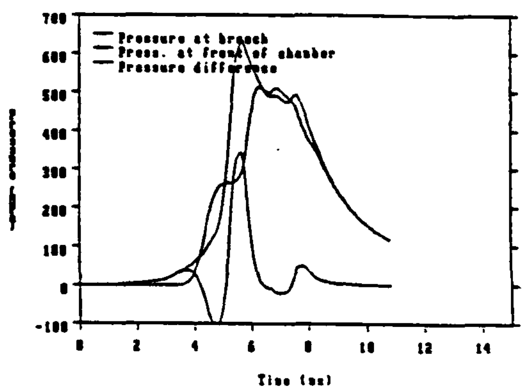

{g,g}/[bn|nn]/wk imp

where: st imp = strong impermeable interface
wk imp = weak impermeable interface

Figure 9. <u>Pressure Data for Basepad Ignition at Breech End. [bn|nn]</u>

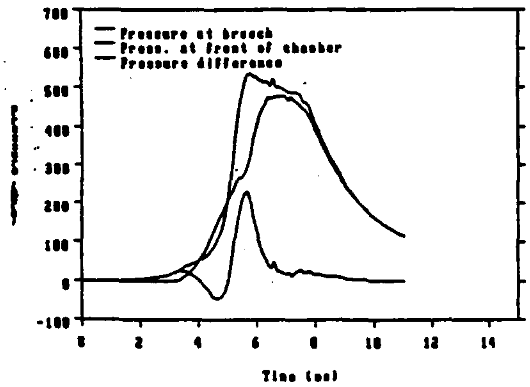

(g,s)/[bn|nn]/st imp

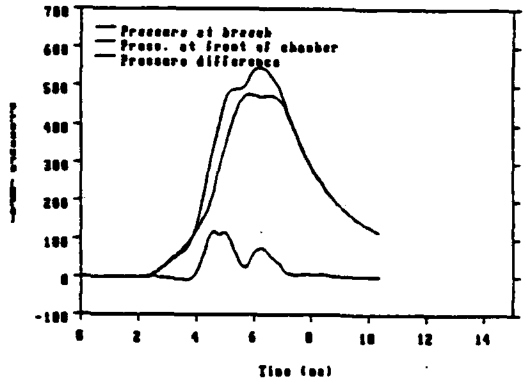

(s,g)/[nn|bn]/st imp

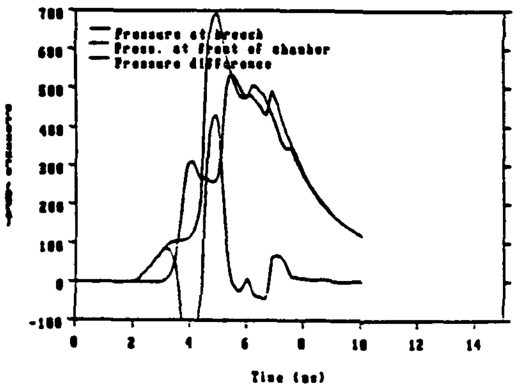

(g,g)/[nb|nn]/st imp

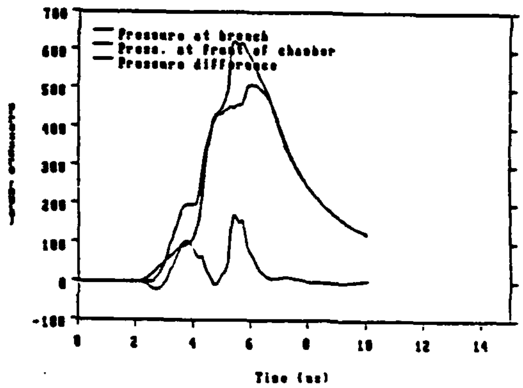

(g,g)/[nn|bn]/st imp

Figure 10. <u>Pressure Data for A Granular Charge With Ignition Occurring at Its Rear End. [bn|nn] and [nn|bn]</u>

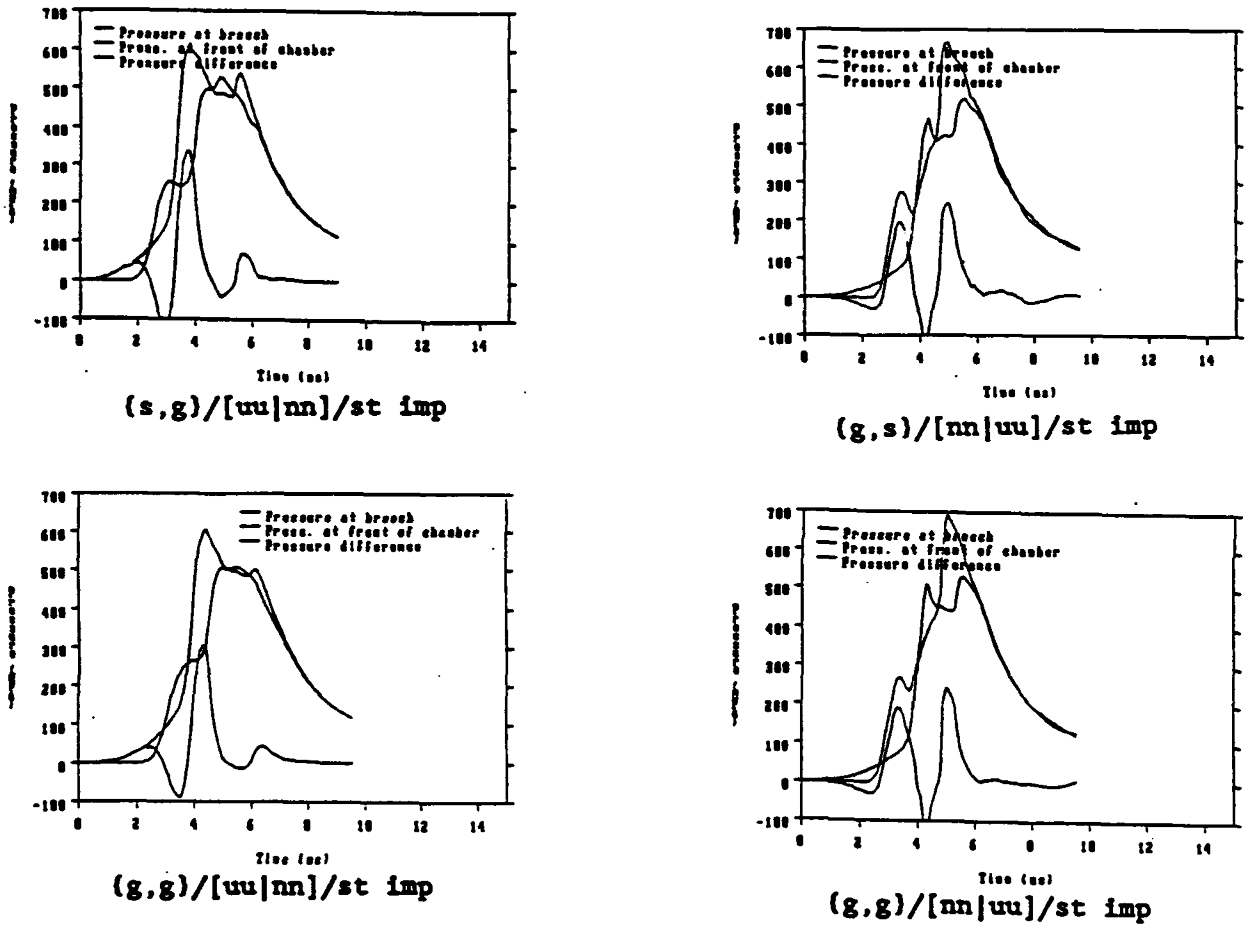

Figure 11. <u>Pressure Data for A Granular Charge Ignited by Adjacent Charge, [uu|nn] and [nn|uu]</u>

3.2.3 Effects of Interface Properties. The data in Tables 2 and 3 show that the interface properties play a key role in the formation of pressure waves. In some cases, the strength of the interface is a dominant factor (see

Figure 12); in other cases, its permeability is the dominant one (see Figure 13). From Appendixes B through E, such dominance is seen only in the charge configurations with one or two granular charges; i.e., (s,g), (g,s), or (g,g). It seems that whether the strength or the permeability is the dominant property depends on the granulation in the cartridge component which has no ignition source initially.

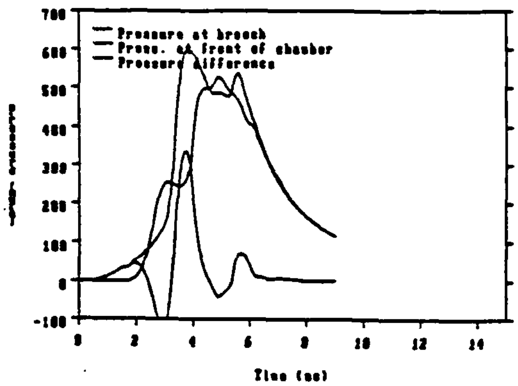

(s,g)/[uu|nn]/st imp

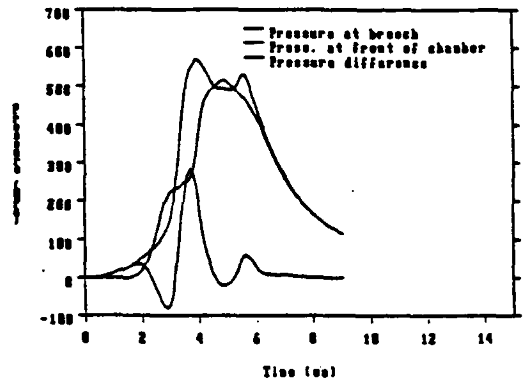

(s,g)/[uu|nn]/wk imp

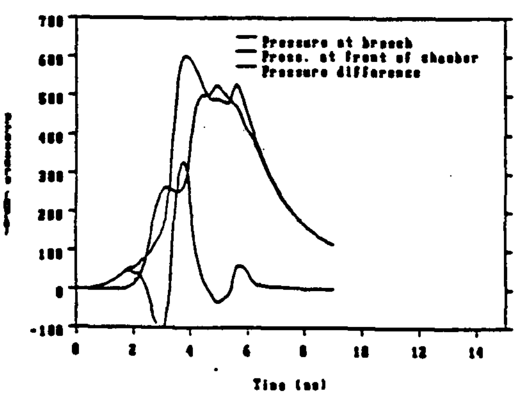

(s,g)/[uu|nn]/st per

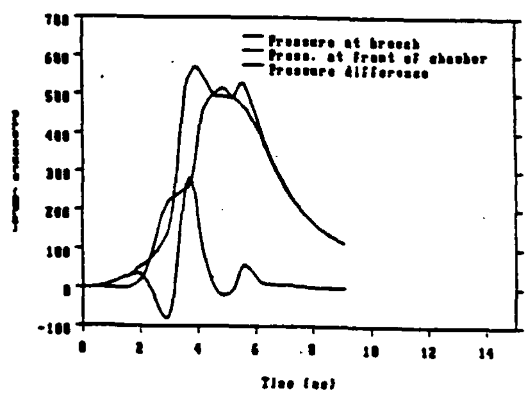

(s,g)/[uu|nn)/wk per

where: st imp = strong impermeable interface
wk imp = weak impermeable interface
st per = strong semi-permeable interface
wk per = weak semi-permeable interface

Figure 12. Effect of Interface Strength

(s,g)/[nb|bn]/wk per

(s,g)/[nb|nn]/no no

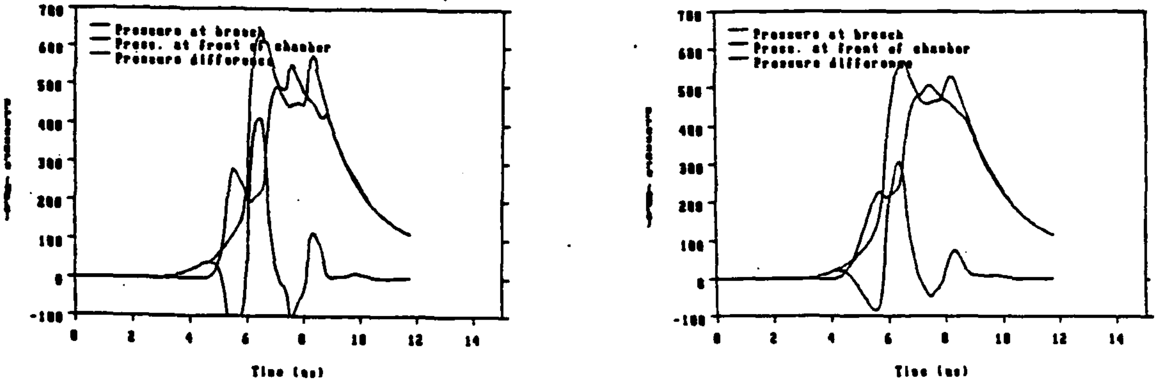

(s,g)/[nb|nn]/st imp

(s,g)/[nb|nn]/st per

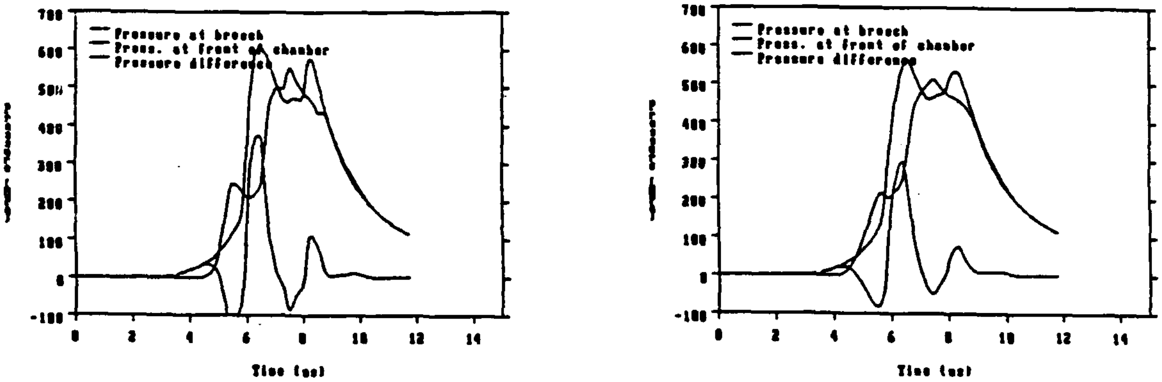

(s,g)/[nb|nn]/wk imp

(s,g)/[nb|nn]/wk per

Figure 13. Effect of Interface Permeability

4. CONCLUSIONS

The charge configuration (s,s) is the most forgiving system allowing the most arrangements of igniter location than any of other charge configurations.

Uniform ignition along the entire charge length produces good ballistic behavior in all of the charge configurations. Center ignition is also a good ignition scheme for the charge configuration (s,s).

In the case that a basepad at the breech end is the only ignition source (i.e., [bn|nn] ignition), high-amplitude pressure waves result in the charge configurations (s,g), (g,s), and (g,g). In the charge configuration (s,s), the pressure waves are moderate, however, the intergranular stress is very high.

The most fault tolerant ignition system may be base ignition of the forward charge with stick propellant in the rear charge, i.e., the charge configurations (s,s) and (s,g).

The cartridge with a granular charge as its component may experience high-amplitude pressure waves or a high intergranular stress or both if there is only one basepad as the ignition source of the charge or if the charge has no direct ignition source at all.

The flow barrier across the cartridge case interface is a major factor in the formation of pressure waves. Its shear strength, permeability, and duration of rupturing are all critically important in the present calculations. These data should be accurately characterized in order to quantitatively predict the interior ballistic performance of a two-piece cartridge.

5. REFERENCES

Chang, L.M. "Numerical Simulation of Interior Ballistic Phenomena in a Gun System." AIAA Paper No. 90-2068, July 1990.

Chang, L.M., R.W. Deas, and J. Grosh. "Ignition Studies of Two-Piece Cartridges for an Advanced Tank Cannon System (ATACS)." BRL-TR-3249, U.S. Army Ballistic Research Laboratory, Aberdeen Proving Ground, MD, August 1991.

Gough, P.S. "The XNOVAKTC Code." BRL-CR-627, U.S. Army Ballistic Research Laboratory, Aberdeen Proving Ground, MD, February 1990.

Horst, A.W. "Breechblow Phenomenology Revisited." BRL-TR-2707, U.S. Army Ballistic Research Laboratory, Aberdeen Proving Ground, MD, January 1986.

Lieb, J.R.. "Bed Testing of Gun Propellants at High Strain." 1991 JANNAF Structure and Mechanical Behavior Subcommittee Meeting, CPIA Publication 566, pp 243, May 1991.

May, I.W. and A.W. Horst. "Charge Design Considerations and Effect on Pressure Waves in Gun." ARBRL-TR-0227, U.S. Army Ballistic Research Laboratory, Aberdeen Proving Ground, MD, December 1978.

APPENDIX A

A Typical Input Data File

Charge Configuration: (s,g); Ignition: [nb|bn]; Interface: strong/permeable

```
GENERIC TWO PIECE CARTRIDGE STICK-gran inter base  str per sgibsp
TFFFTTT          1 6      00010      0
75    150000    15000           .001
0.100       254.55      .00002      2.5         .05         .01         .0001       .0001
6     0     0     4     0     0     2     2     0     0     0     8
0     0
530.        14.7        29.000      1.4
530.
JA2 19P CYL NOMIN       0.0         19.00       16.         .056355
-9    .72         .029        .75         19.0                                              1
1.0         0.1         0.0         0.0         0.0         0.1
30000.      1.0         50000.                  .5
10000.      .001868     .7939       100000.     .0005363    .9294       0.0         800.
0.0277      .0001345    .6
20293046. 24.876        1.2272      26.86
JA2 19P CYL NOMIN       19.00       42.25       18.         .056355
 9    .72         .029        .75         19.0                                              0
3000.       1.0         50000.                  .5
10000.      .001868     .7939       100000.     .0005363    .9294       0.0         800.
0.0277      .0001345    .6
20293046. 24.876        1.2272      26.86
28552494. 25.93         1.1311      24.3
0.00        2.5         2.97        3.10        25.1        3.10        40.017      3.10
43.809      2.855       295.684     2.855
0.0         150.        .4660       2100.0      1.066       250.0       253.866     0.0
1.4         14.7        530.        29.0
0.1         0.3         2.3125      2.3125
4.75        .012        .15
42.25       30.00       96.         0.0
0.0         39.45       15.45       27.45       3.75        57.95        145.95      39.45
0     0
3     2     0     0     1     5     3     1
0.0         .656        6.125       .656        18.685      1.375
2     4
0.0         0.1378      42.25       0.1378
0.0332      14.7        0.0455      11000.      0.0497      25000.      .0548       100000.
2
40000.      0.000137    1.301       100000.     8.515E15    -3.
0.0         500.        0.0277      .0001345    0.6
9420000.    23.00       1.25
    1     1 3143      3     0     0
100.        1000.0      .5
100.        500.        .5
50.         1000.       .5
50.         500.        .5
0.0         0.0         0.0
0     0     3
0.0332      9420000.    23.00       1.25        .25
2.3         0.0         3.8         3.00        5.3         0.0
    0     0     3
0.06         5500000.   35.         1.2187      .25
0.0          0.0        3.75        2.67        7.5          0.0
    0     0     3
0.06         5500000.   35.         1.2187      .25
0.0          0.0        3.75        1.78        7.5          0.0
0     0     3
0.0332      9420000.    23.00       1.25        .25
1.1         0.0         2.6         6.00        4.1         0.0
```

APPENDIX B

Plots of Pressure-Times Traces for the Charge Configuration (s,s)

See Table 1 for the representations of the symbols [uu|uu],[uu|nn], [nn|uu], [bn|bn], [bn|nn], [nn|bn], [nb|bn], and [nb|nn]. The following symbols are defined as:

P_b = pressure at the breech, MPa
P_f = pressure at the forward end of the gun chamber, MPa
$dP = P_b - P_f$, MPa
no no = no interface
st imp = strong impermeable interface
st per = strong permeable interface
wk imp = weak impermeable interface
wk per = weak permeable interface

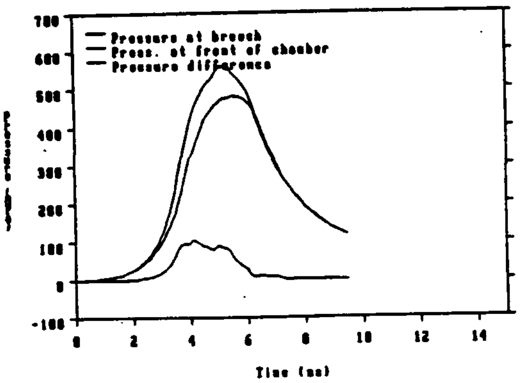

(s,s)/[uu|uu]/no no

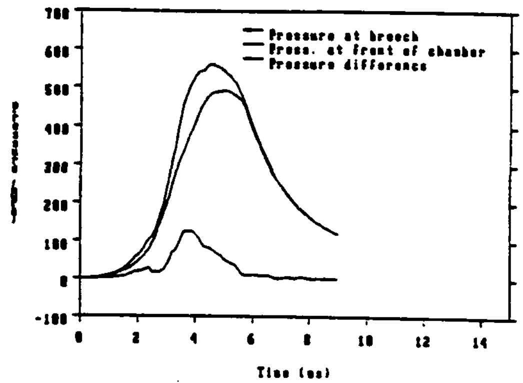

(s,s)/[uu|uu]/st imp

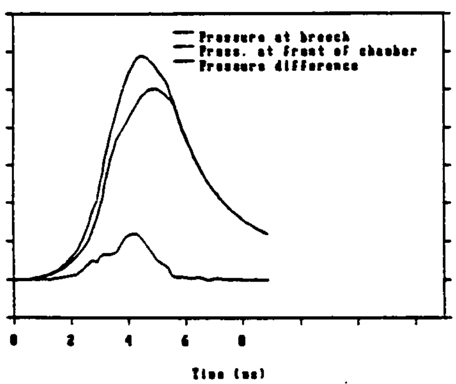

(s,s)/[uu|uu]/st per

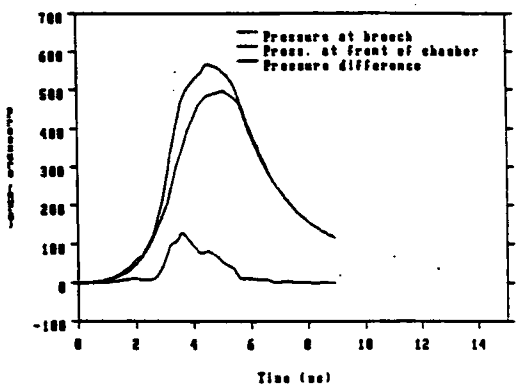

(s,s)/[uu|uu)/wk imp

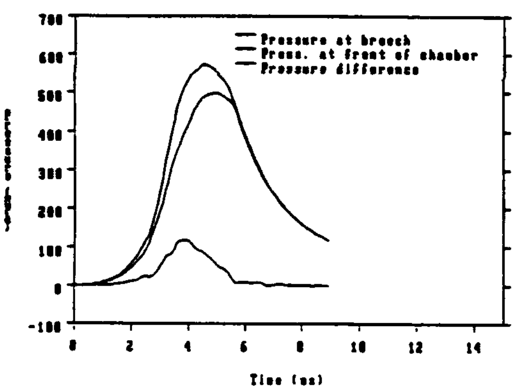

(s,s)/[uu|uu]/wk per

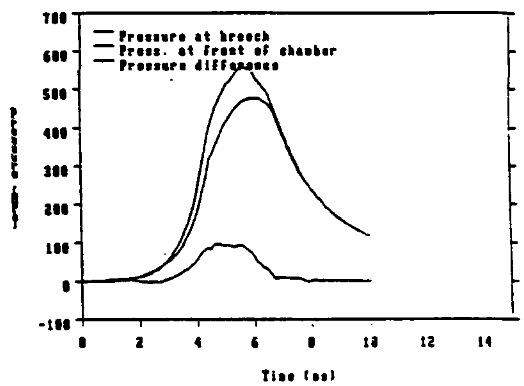

(s,s)/[uu|nn]/ no no

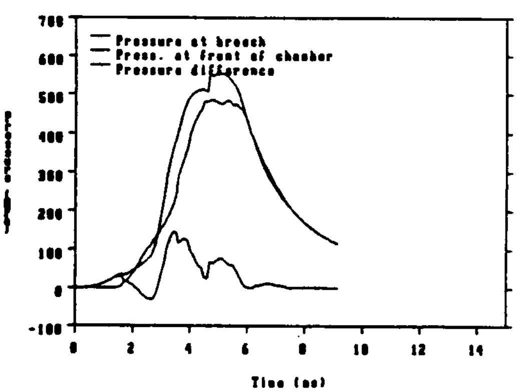

(s,s)/[uu|nn]/st imp

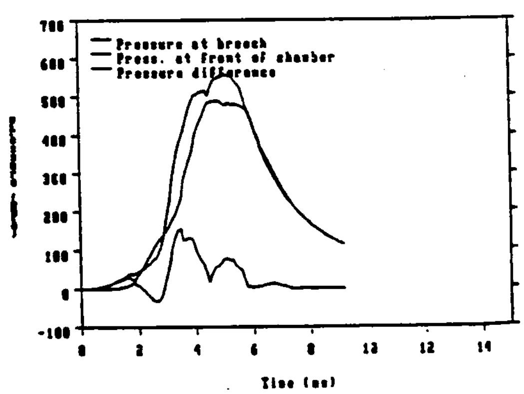

(s,s)/[uu|nn]/st per

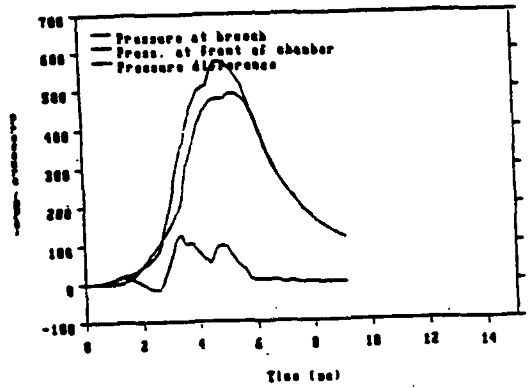

(s,s)/[uu|nn]/wk imp

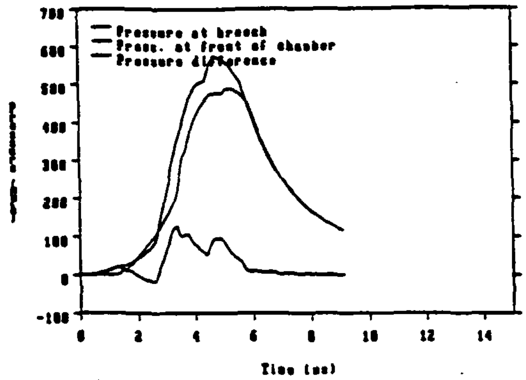

(s,s)/[uu|nn]/wk per

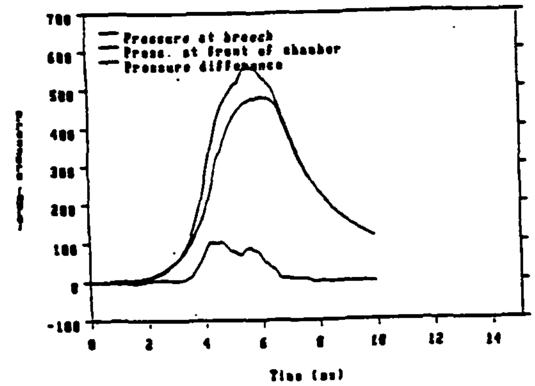

(s,s)/[nn|uu]/no no

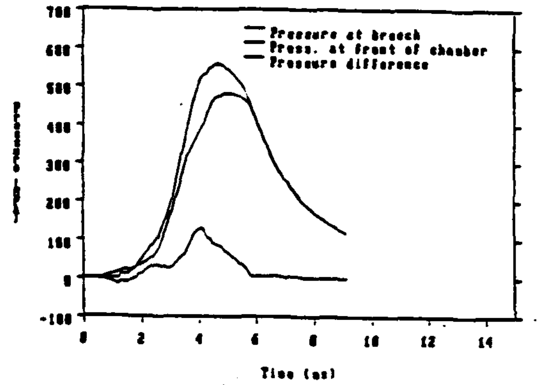

(s,s)/[nn|uu]/st imp

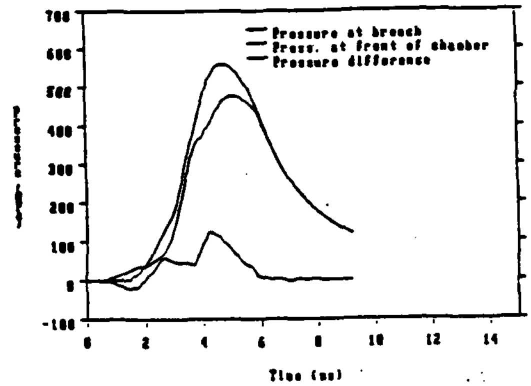

(s,s)/[nn|uu]/st per

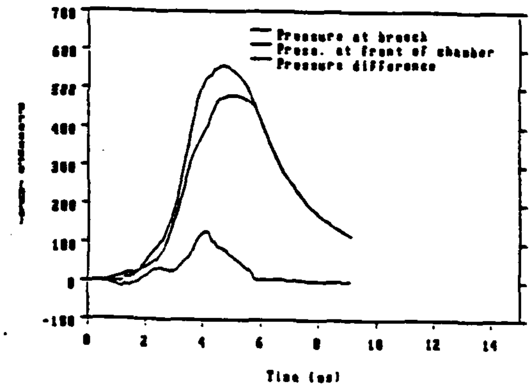

(s,s)/[nn|uu]/wk imp

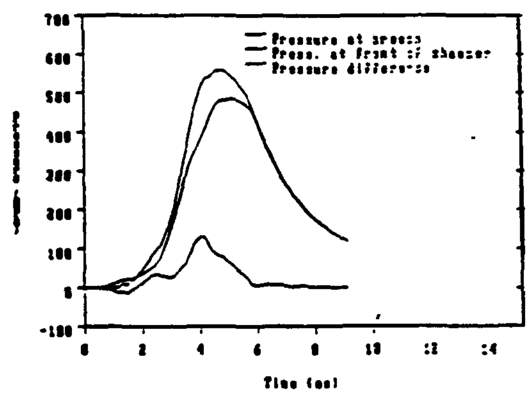

(s,s)/[nn|uu]/wk per

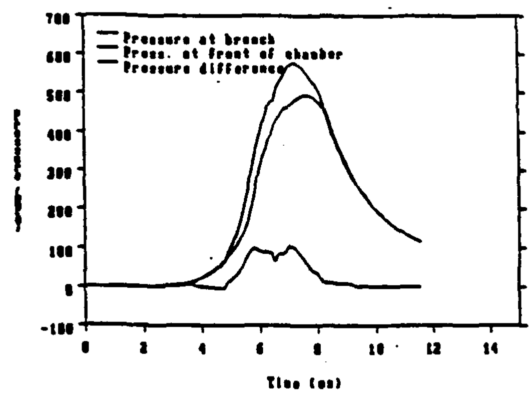

(s,s)/[bn|bn]/no no

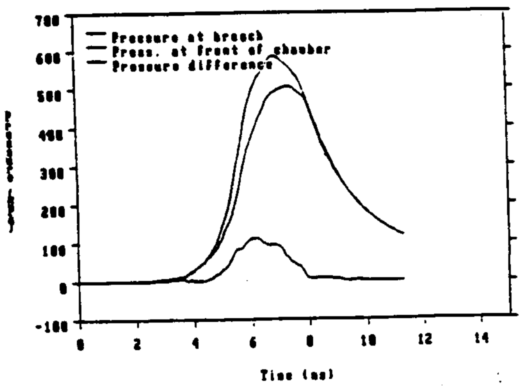

(s,s)/[bn|bn]/st imp

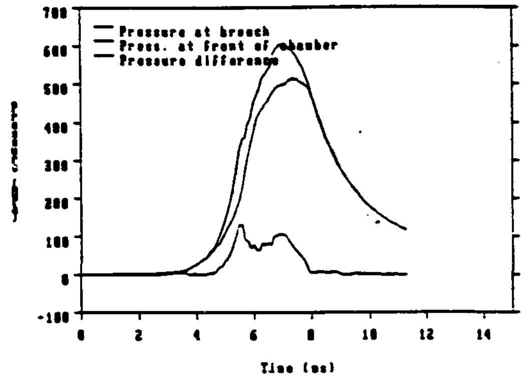

(s,s)/[bn|bn]/st per

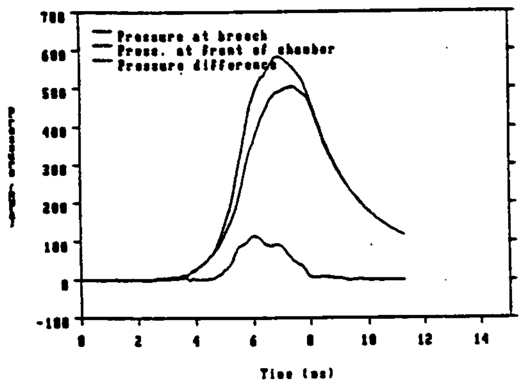

(s,s)/[bn|bn]/wk imp

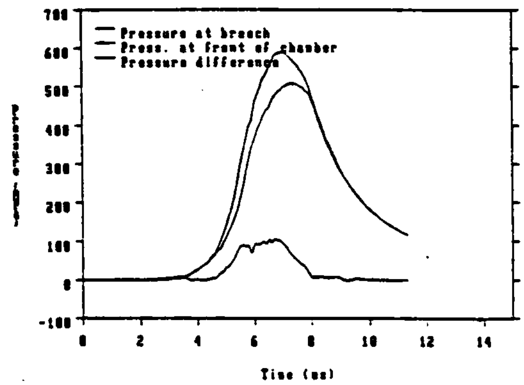

(s,s)/[bn|bn]/wk per

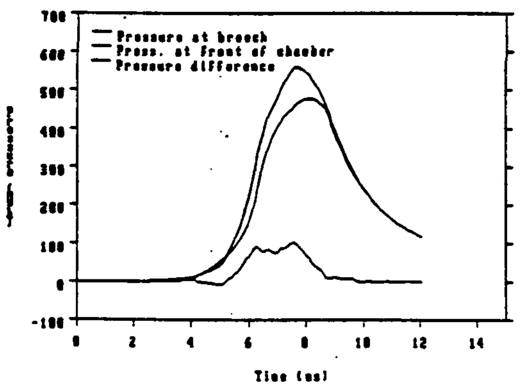

(s,s)/[bn|nn]/no no

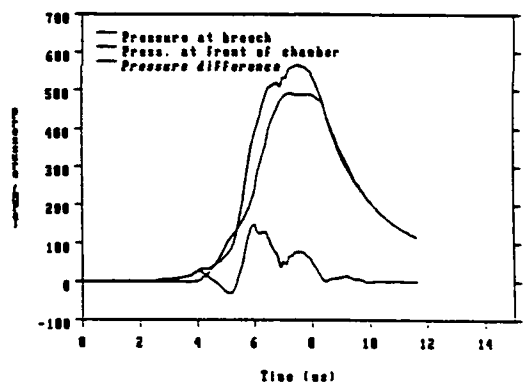

(s,s)/[bn|nn]/st imp

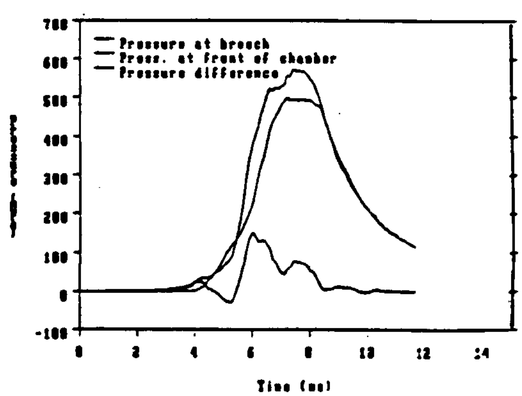

(s,s)/[bn|nn]/st per

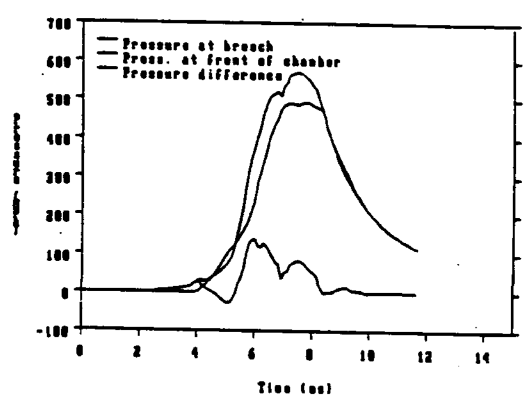

(s,s)/[bn|nn]/wk imp

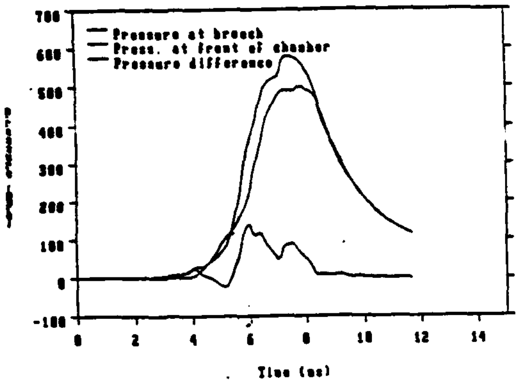

(s,s)/[bn|nn]/wk per

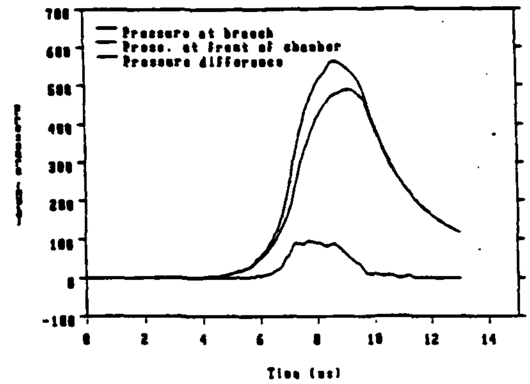

(s,s)/[nn|bn]/no no

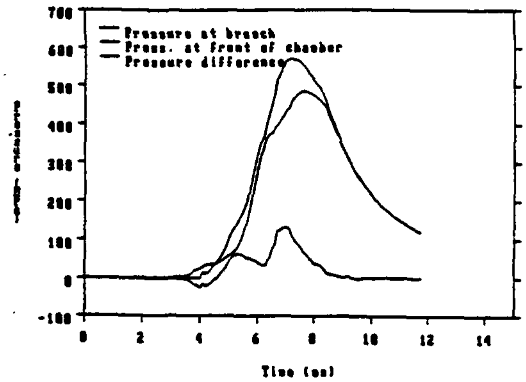

(s,s)/[nn|bn]/st imp

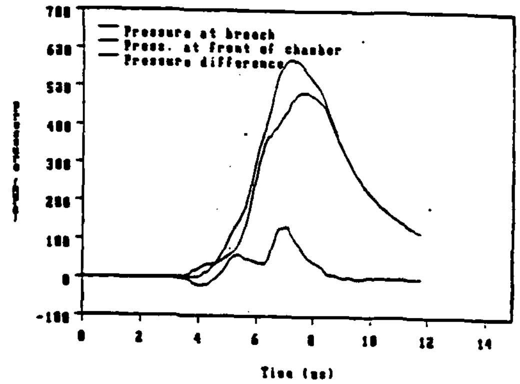

(s,s)/[nn|bn]/st per

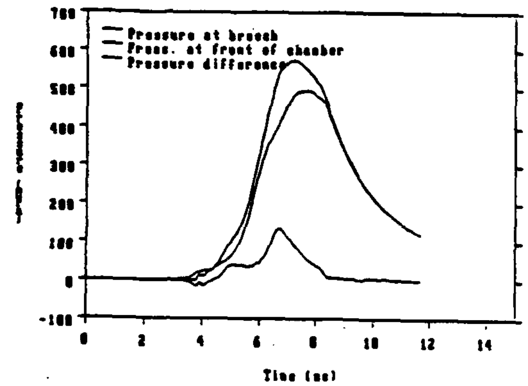

(s,s)/[nn|bn]/wk imp

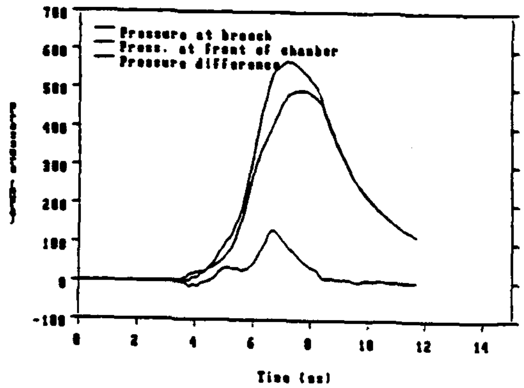

(s,s)/[nn|bn]/wk per

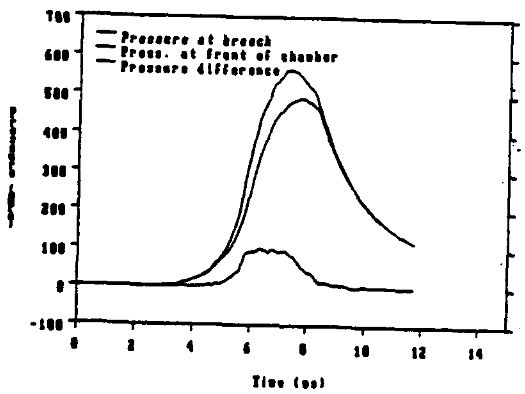

(s,s)/[nb|bn]/no no

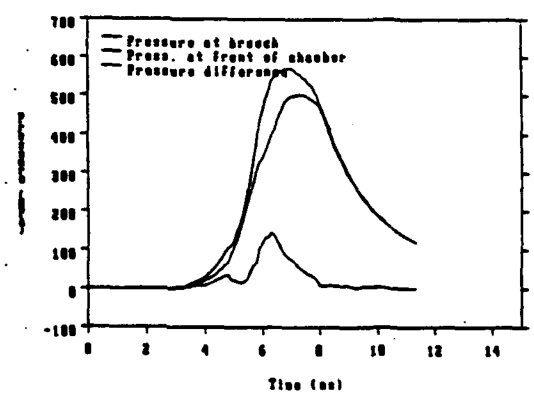

(s,s)/[nb|bn]/st imp

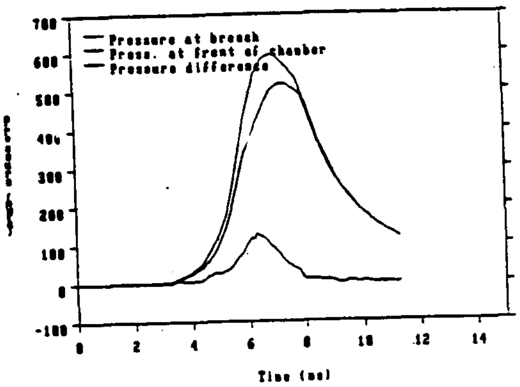

{s,s}/[nb|bn]/st per

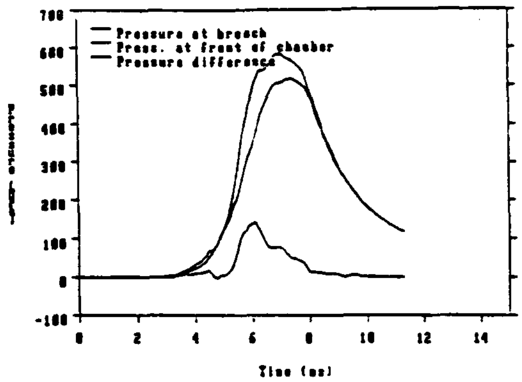

{s,s}/[nb|bn]/wk imp

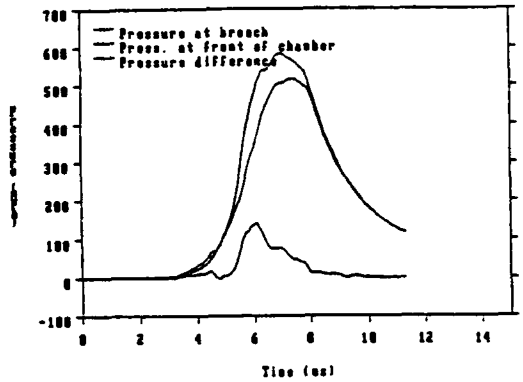

{s,s}/[nb|bn]/wk per

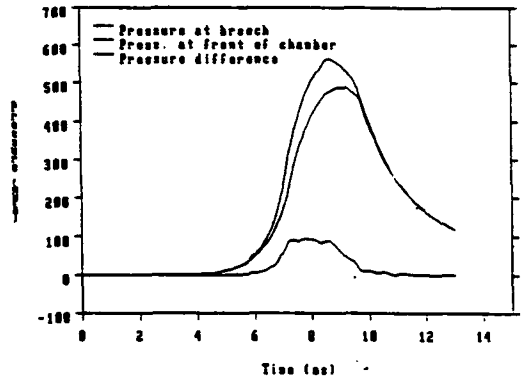

{s,s}/[nb|nn]/ no no

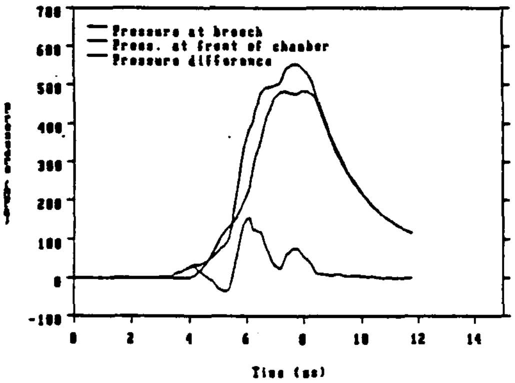

{s,s}/[nb|nn]/st imp

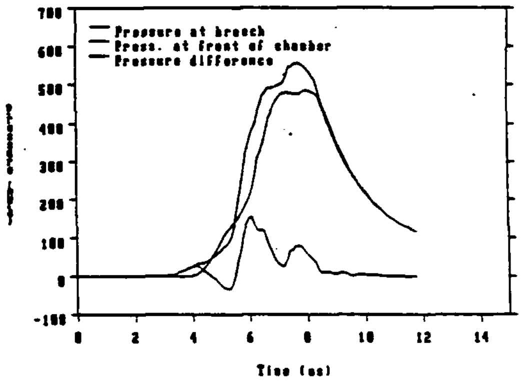

{s,s}/[nb|nn]/st per

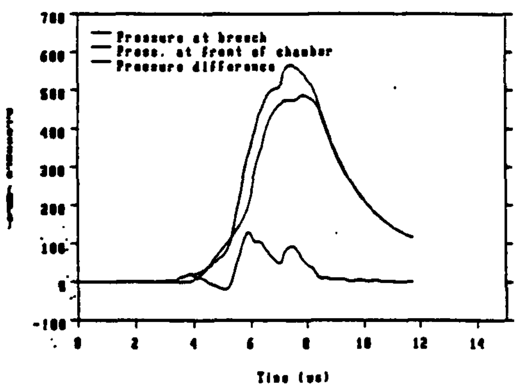

{s,s}/[nb|nn]/wk imp

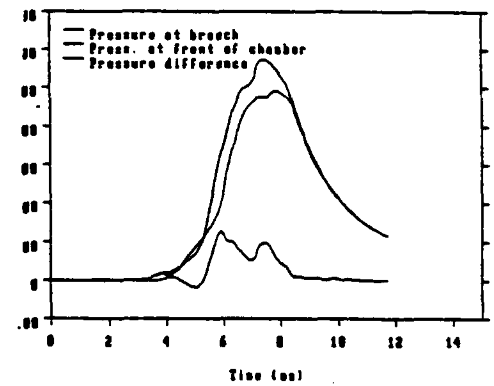

{s,s}/[nb|nn]/wk per

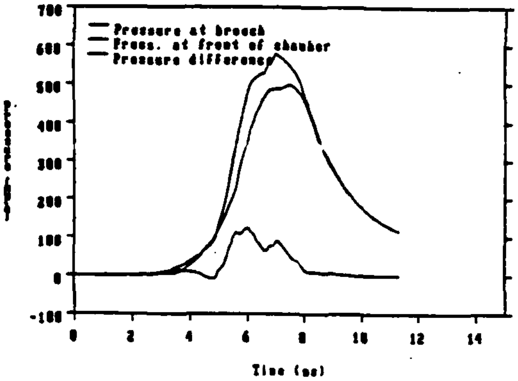

{s,s}/[bb|nn]/no no

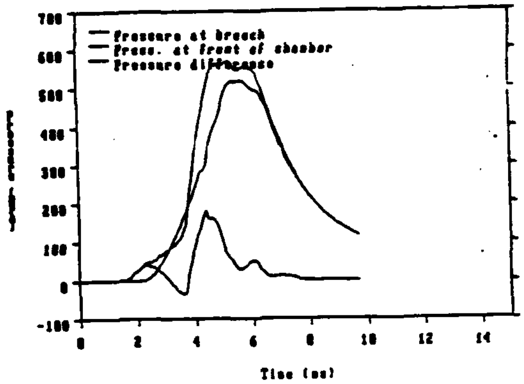

{s,s}/[bb|nn]/st imp

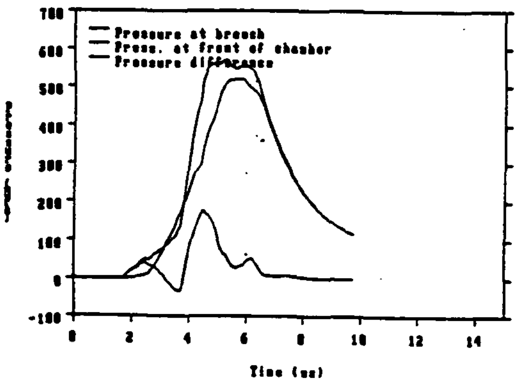

{s,s}/[bb|nn]/st per

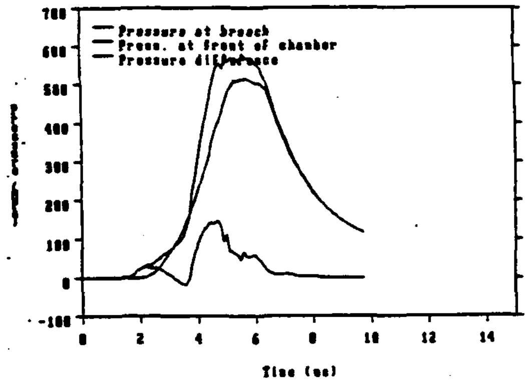

{s,s}/[bb|nn]/wk imp

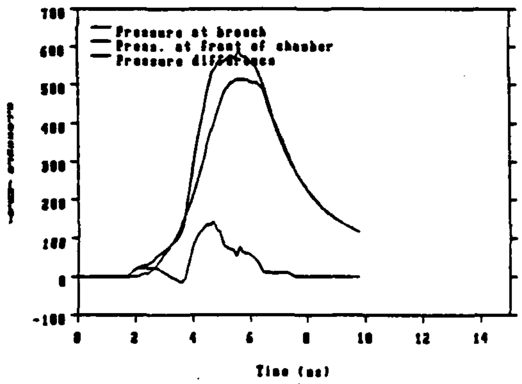

{s,s}/[bb|nn]/wk per

INTENTIONALLY LEFT BLANK.

APPENDIX C

Plots of Pressure-Time Traces for the Charge Configuration (s,g)

See Table 1 and APPENDIX B for the representations of the symbols used.

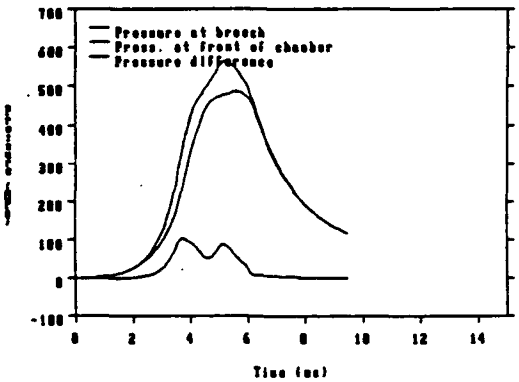

(s,g)/[uu|uu]/no no

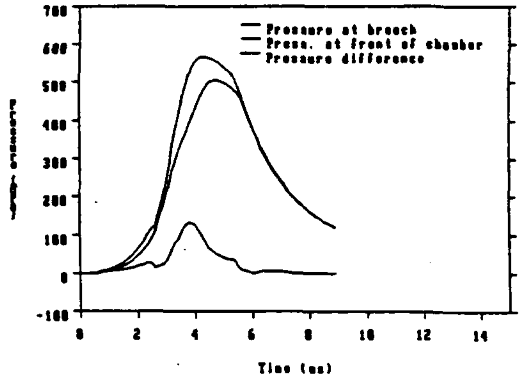

(s,g)/[uu|uu]/st imp

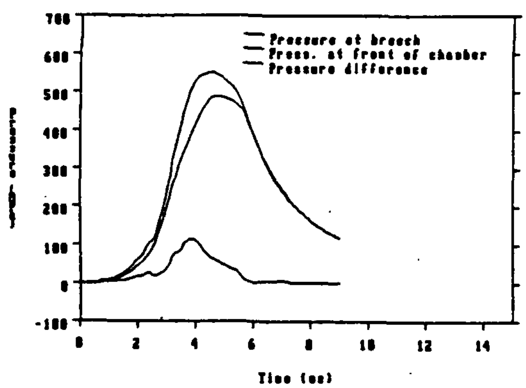

(s,g)/[uu|uu]/st per

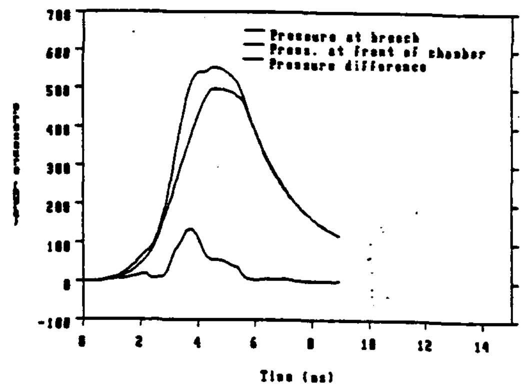

(s,g)/[uu|uu]/wk imp

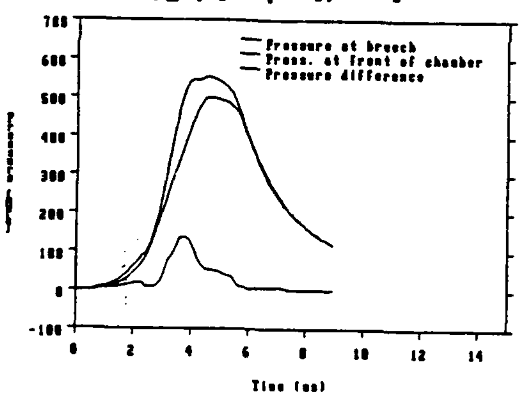

(s,g)/[uu|uu]/wk per

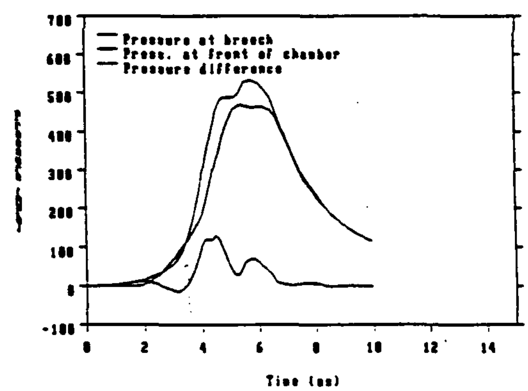

(s,g)/[uu|nn]/no no

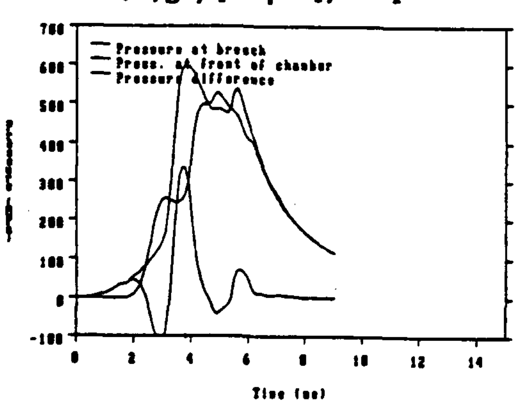

(s,g)/[uu|nn]/st imp

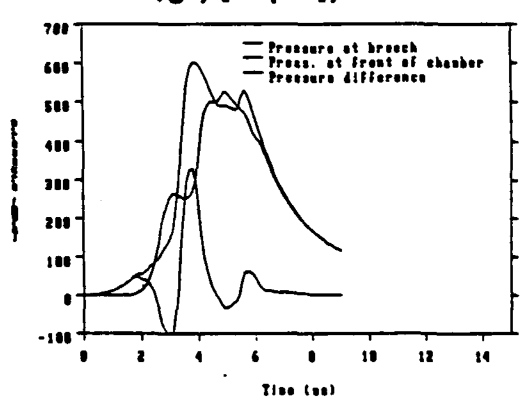

(s,g)/[uu|nn]/st per

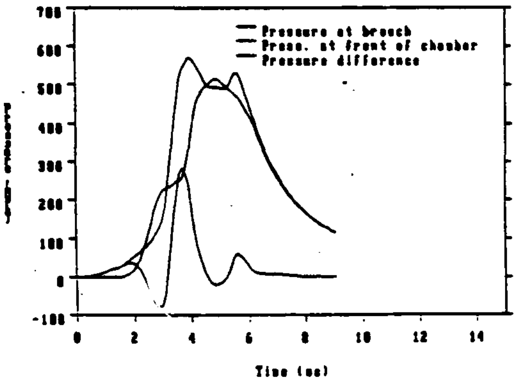

{s,g}/[uu|nn]/wk imp

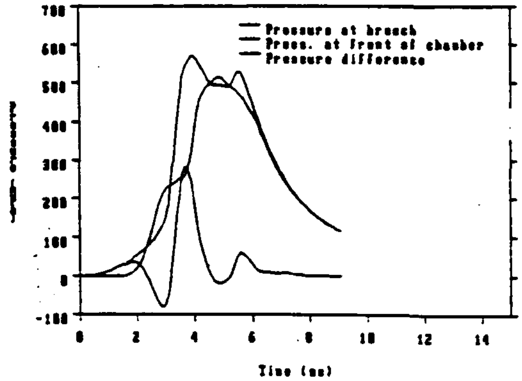

{s,g}/[uu|nn}/wk per

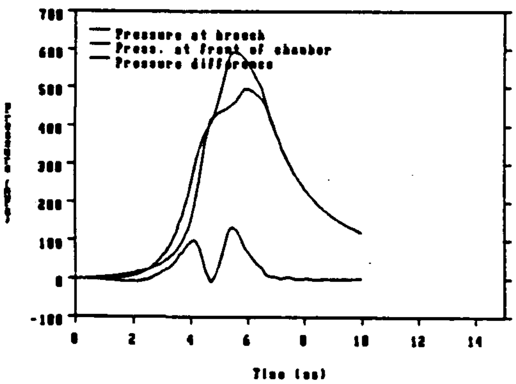

{s,g}/[nn|uu]/no no

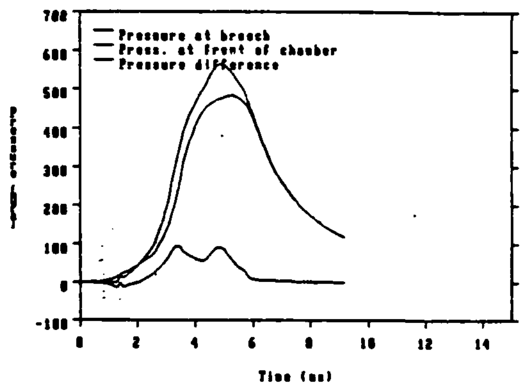

{s,g}/[nn|uu]/st imp

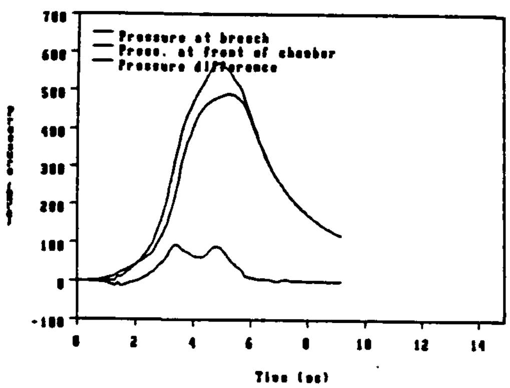

{s,g}/[nn|uu]/st per

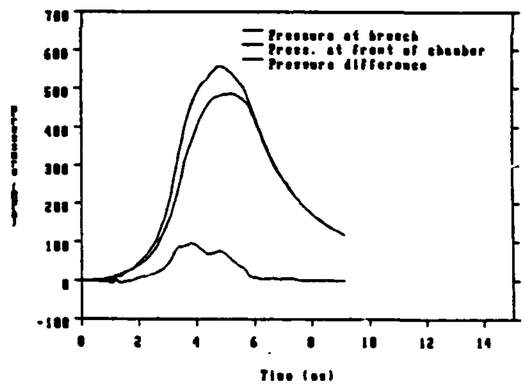

{s,g}/[nn|uu]/wk imp

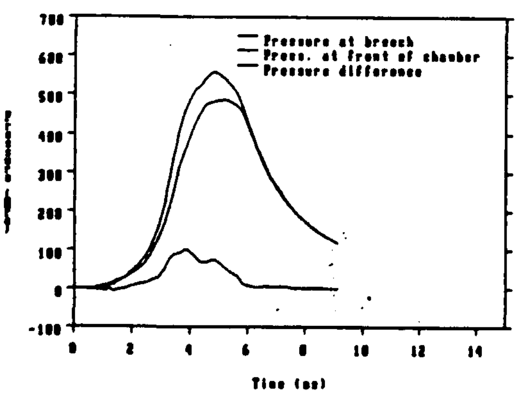

{s,g}/[nn|uu]/wk per

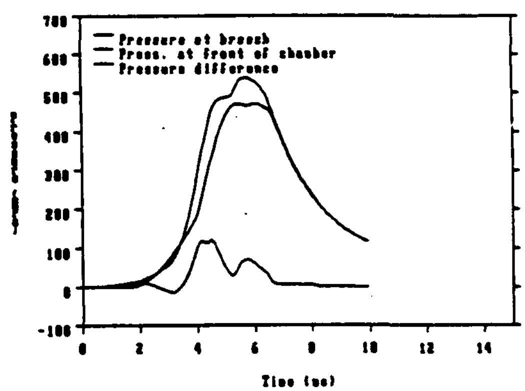

{s,g}/[bn|bn]/no no

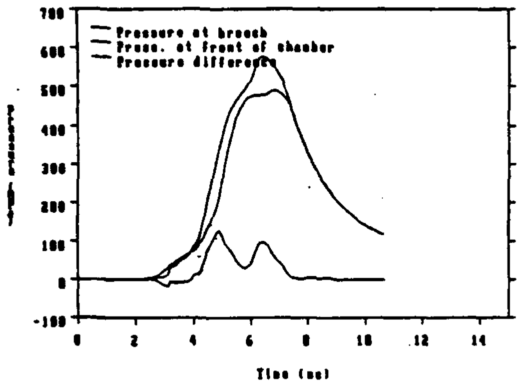

(s,g)/[bn|bn]/st imp

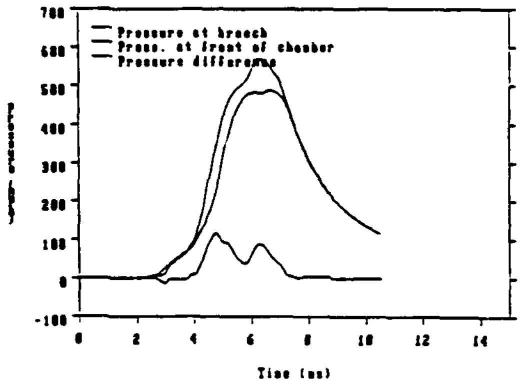

(s,g)/[bn|bn]/st per

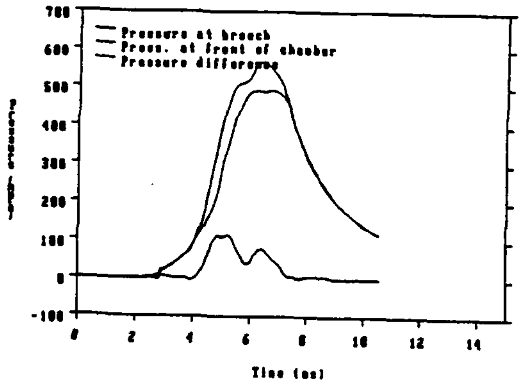

(s,g)/[bn|bn]/wk imp

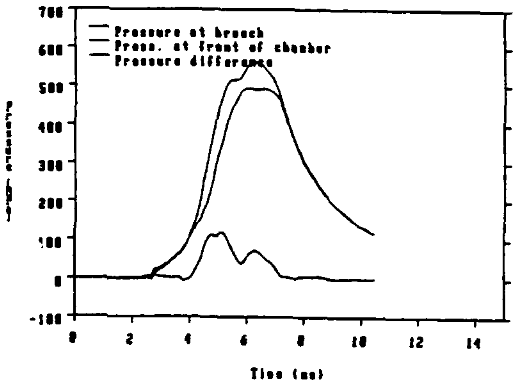

(s,g)/[bn|bn]/wk per

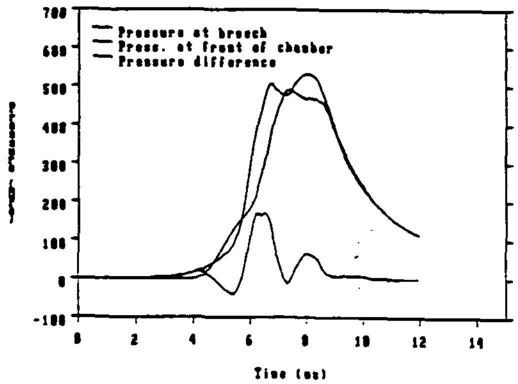

(s,g)/[bn|nn]/no no

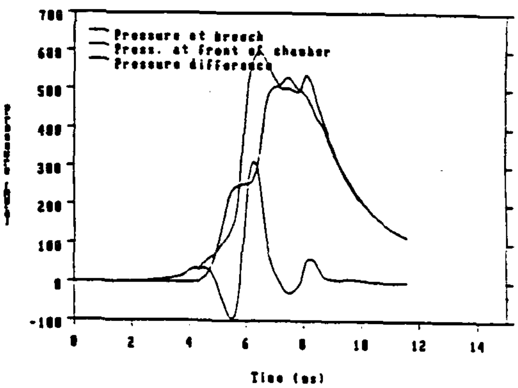

(s,g)/[bn|nn]/st imp

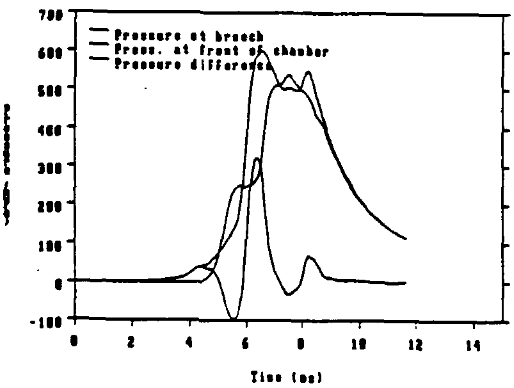

(s,g)/[bn|nn]/st per

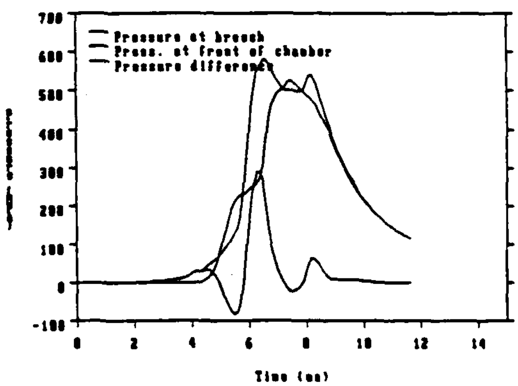

(s,g)/[bn|nn]/wk imp

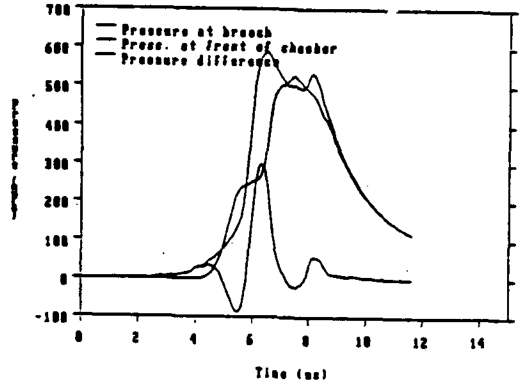

(s,g)/[bn|nn]/wk per

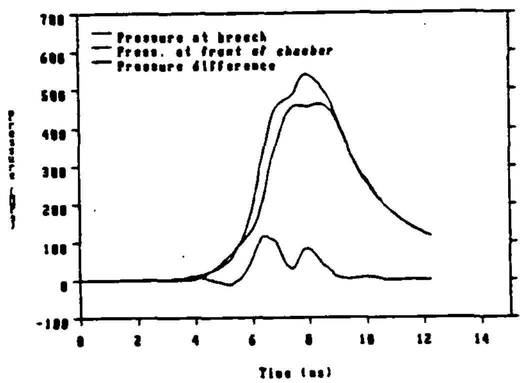

(s,g)/[nn|bn]/no no

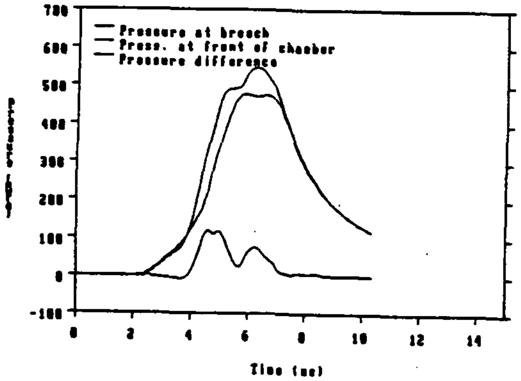

(s,g)/[nn|bn]/st imp

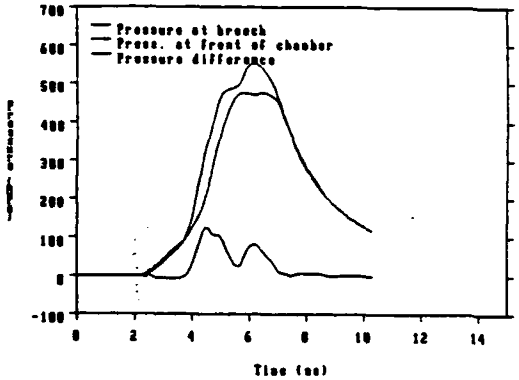

(s,g)/[nn|bn]/st per

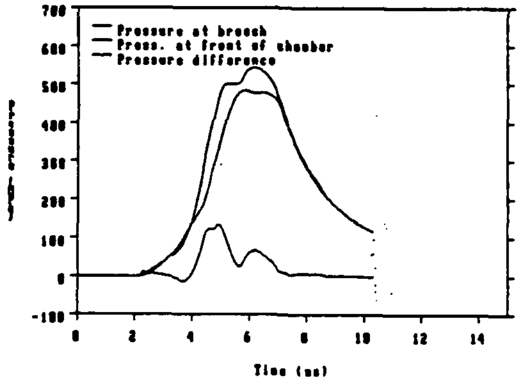

(s,g)/[nn|bn]/wk imp

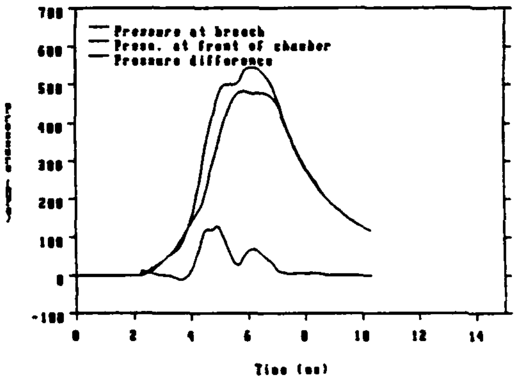

(s,g)/[nn|bn]/wk per

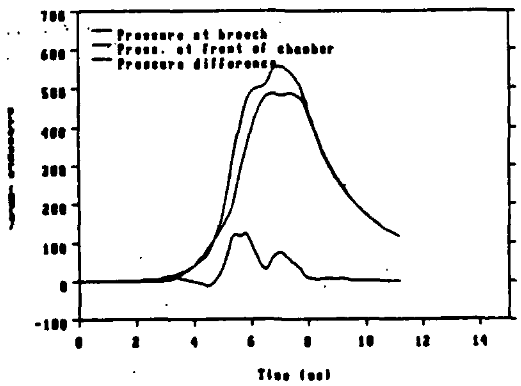

(s,g)/[nb|bn]/no no

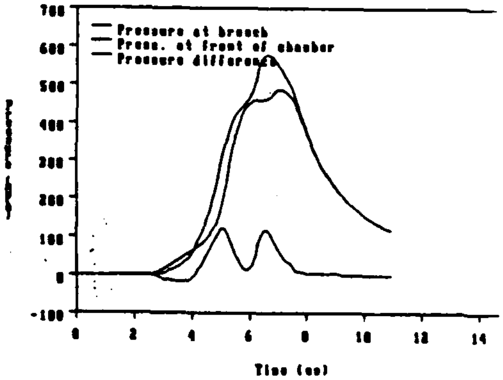

(s,g)/[nb|bn]/st imp

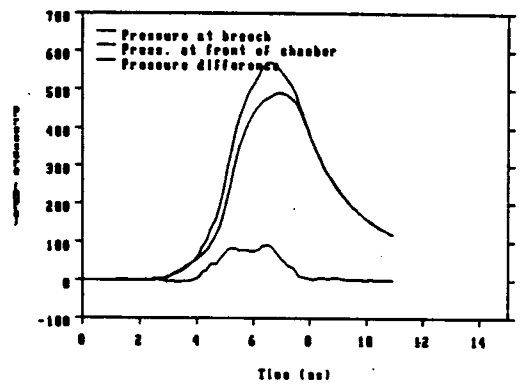

{s,g}/[nb|bn]/st per

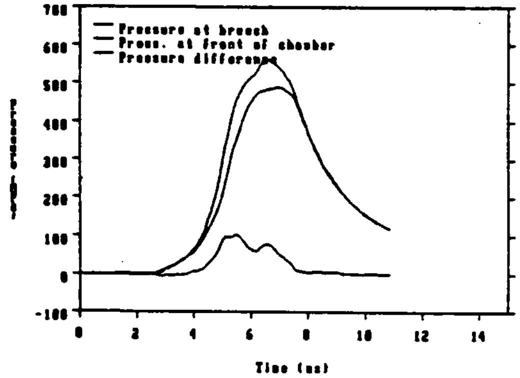

{s,g}/[nb|bn]/wk imp

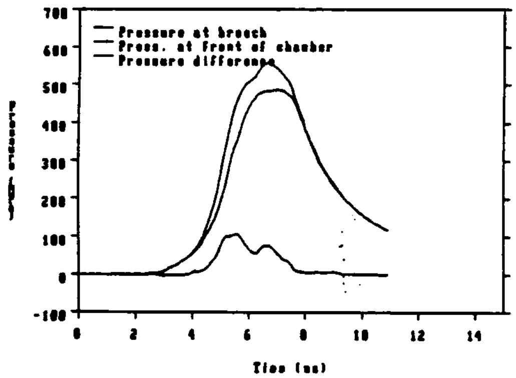

{s,g}/[nb|bn]/wk per

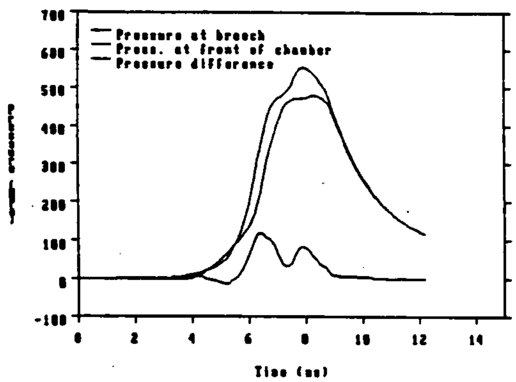

{s,g}/[nb|nn]/no no

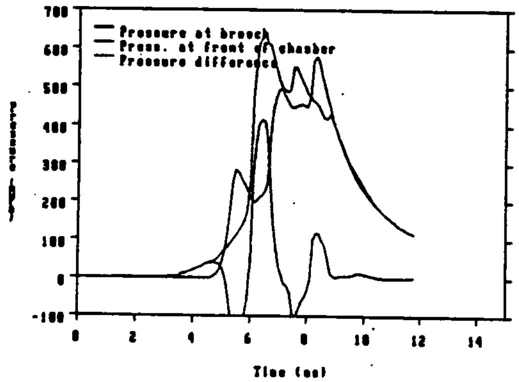

{s,g}/[nb|nn]/st imp

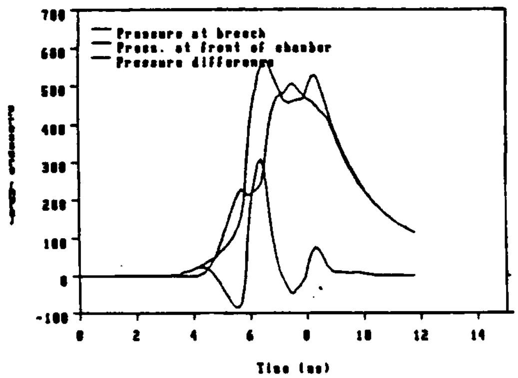

{s,g}/[nb|nn]/st per

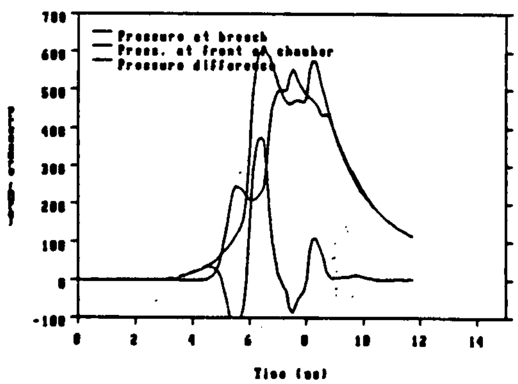

{s,g}/[nb|nn]/wk imp

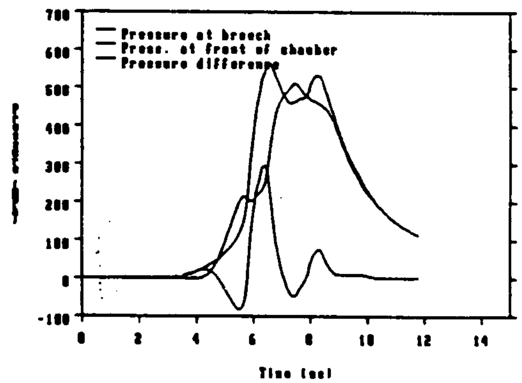

{s,g}/[nb|nn]/wk per

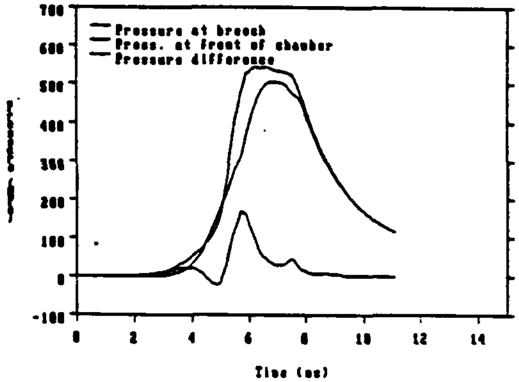

{s,g}/[bb|nn]/no no

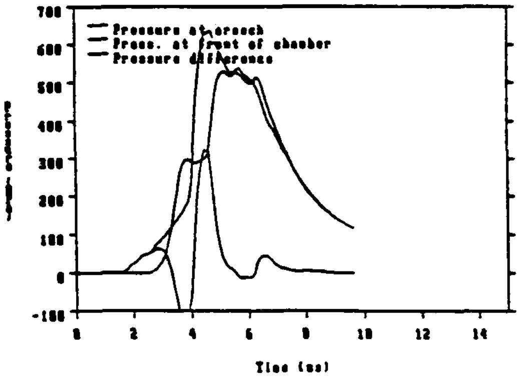

{s,g}/[bb|nn]/st imp

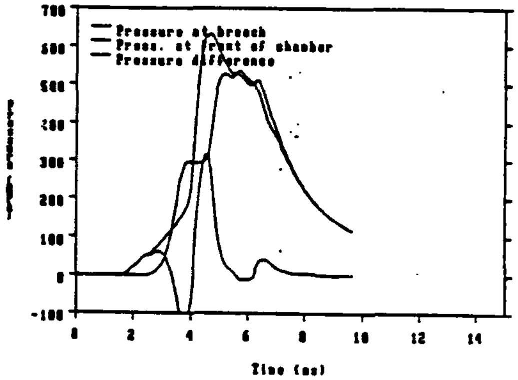

{s,g}/[bb|nn]/st per

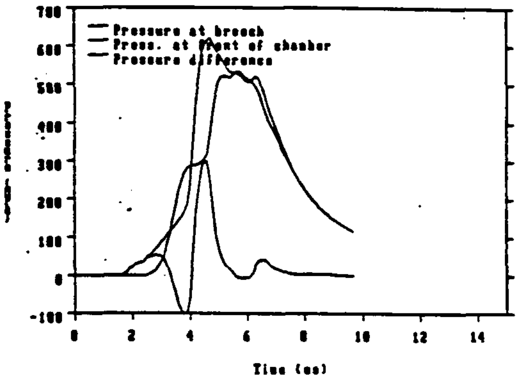

{s,g}/[bb|nn]/wk imp

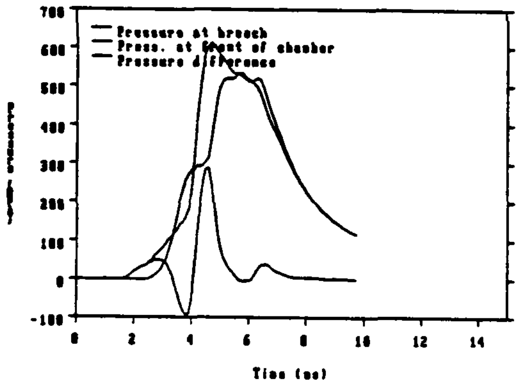

{s,g}/[bb|nn]/wk per

INTENTIONALLY LEFT BLANK.

APPENDIX D

Plots of Pressure-Time Traces for the Charge Configuration (g,s)

See Table 1 and APPENDIX B for the representations of the symbols used.

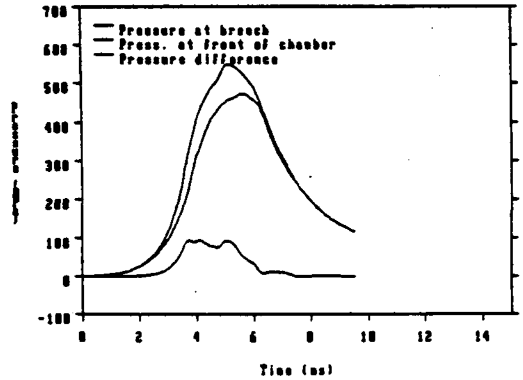

(g,s)/[uu|uu]/no no

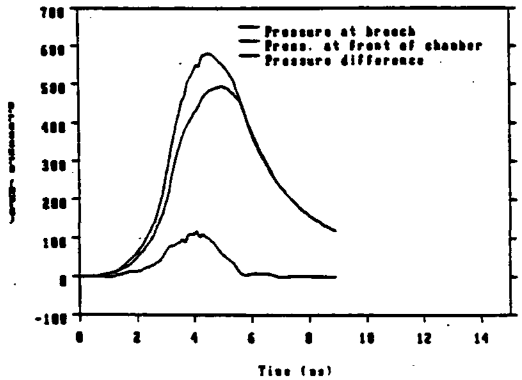

(g,s)/[uu|uu]/st imp

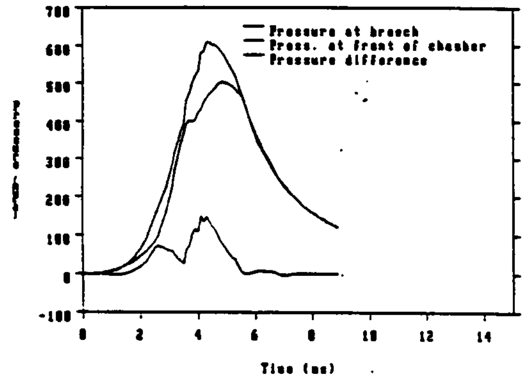

(g,s)/[uu|uu]/st per

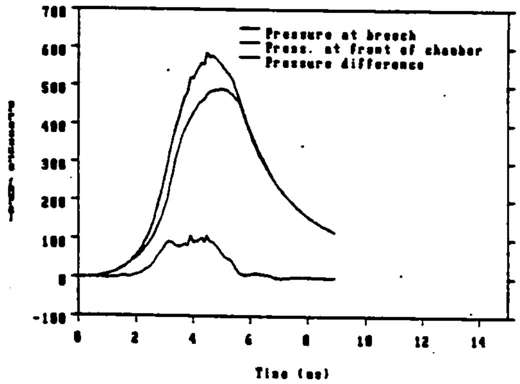

(g,s)/[uu|uu)/wk imp

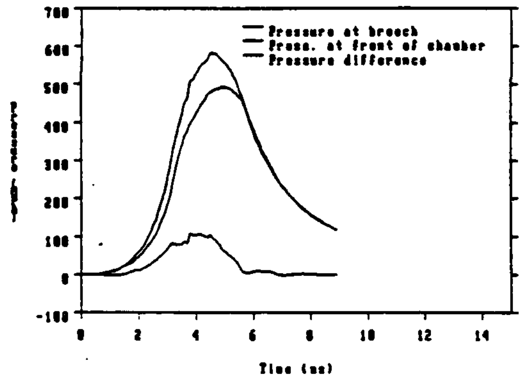

(g,s)/[uu|uu]/wk per

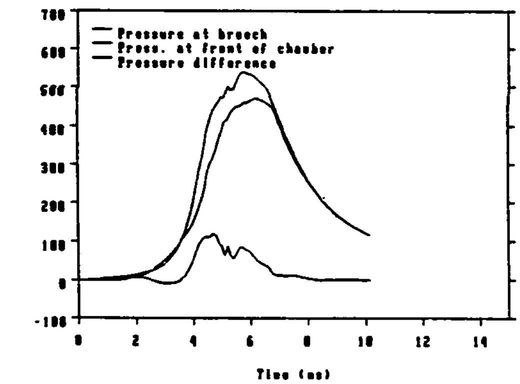

(g,s)/[uu|nn]/ no no

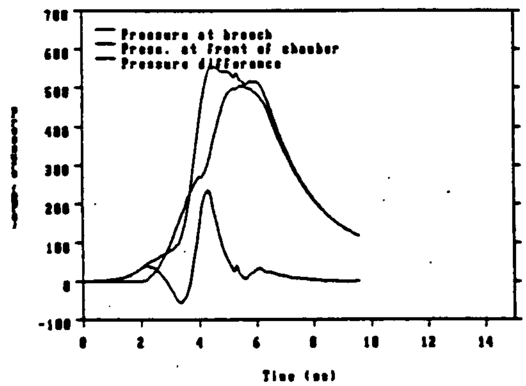

(g,s)/[uu|nn]/st imp

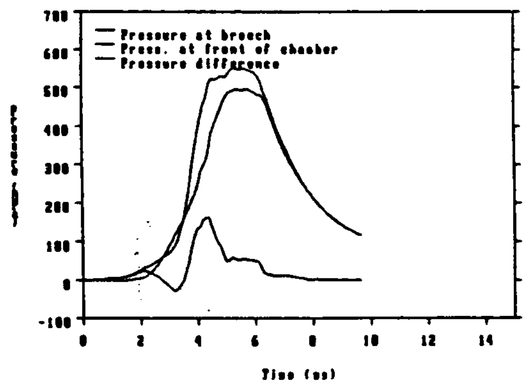

(g,s)/[uu|nn]/st per

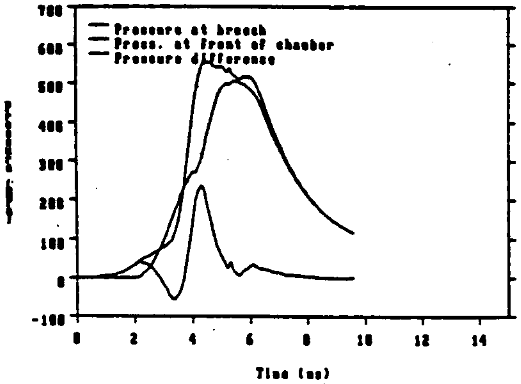

(g,s)/[uu|nn]/wk imp

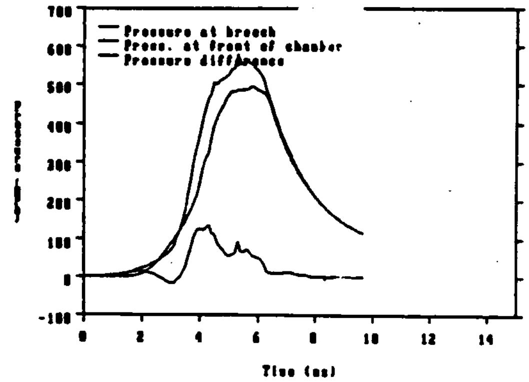

(g,s)/[uu|nn]/wk per

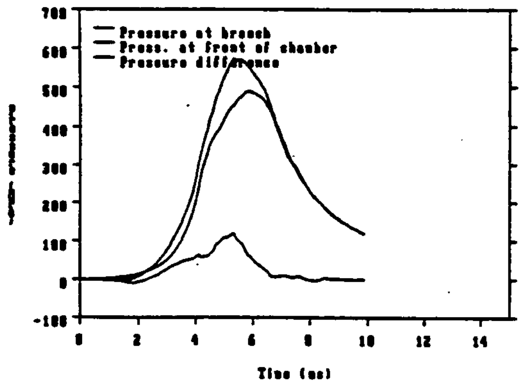

(g,s)/[nn|uu]/no no

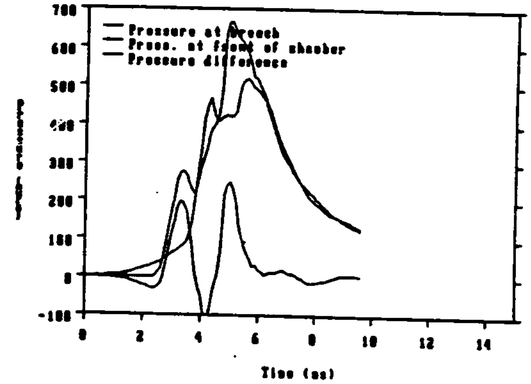

(g,s)/[nn|uu]/st imp

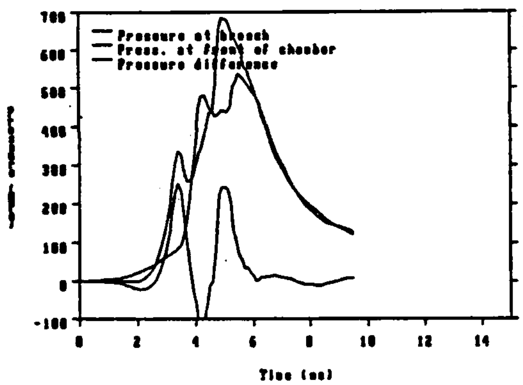

(g,s)/[nn|uu]/st per

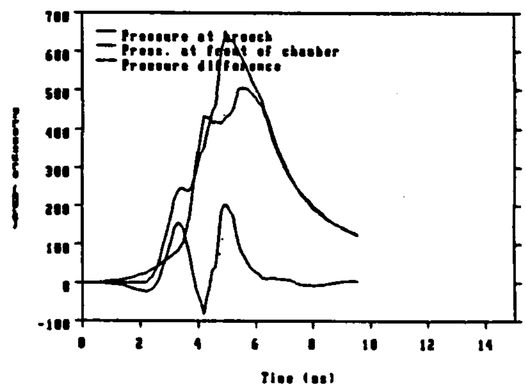

(g,s)/[nn|uu]/wk imp

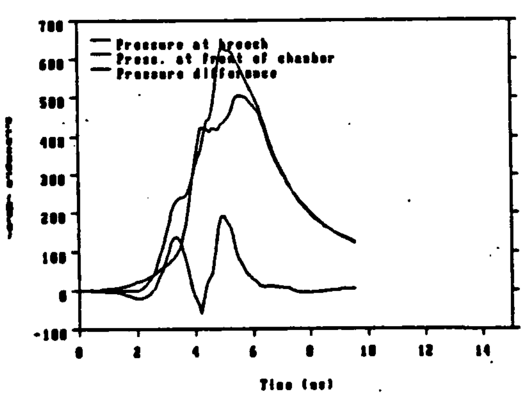

(g,s)/[nn|uu]/wk per

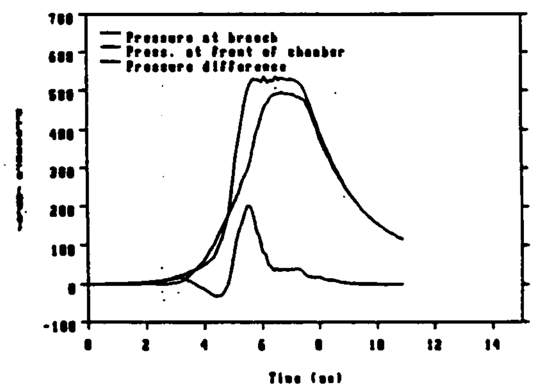

(g,s)/[bn|bn]/no no

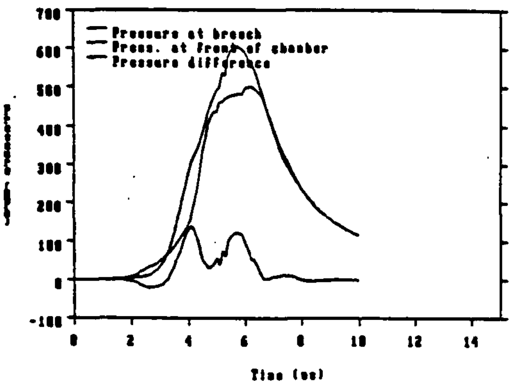

(g,s)/[bn|bn]/st imp

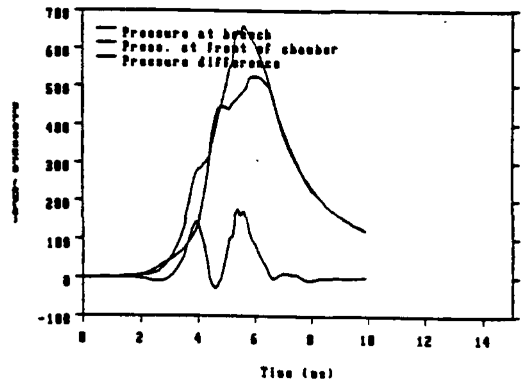

(g,s)/[bn|bn]/st per

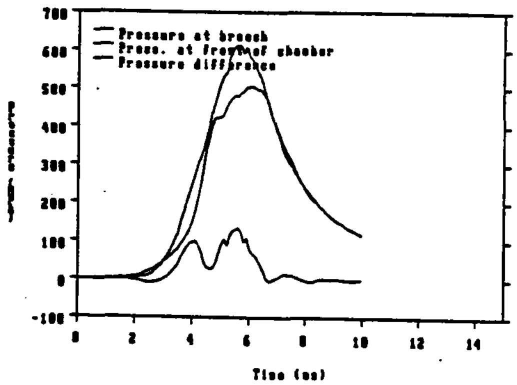

(g,s)/[bn|bn]/wk imp

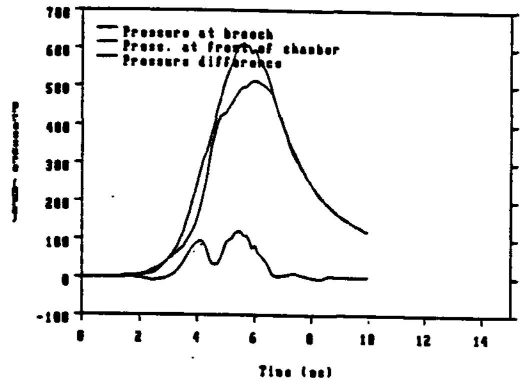

(g,s)/[bn|bn]/wk per

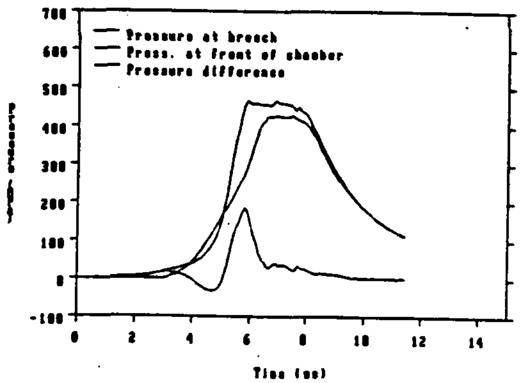

(g,s)/[bn|nn]/no no

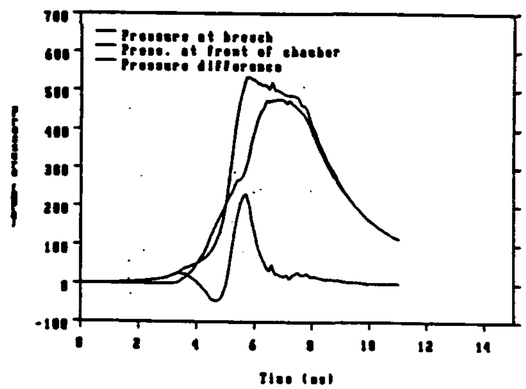

(g,s)/[bn|nn]/st imp

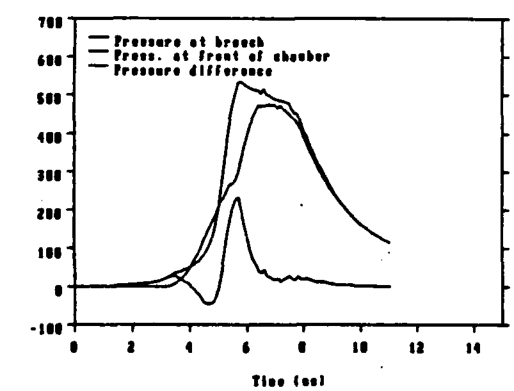

(g,s)/[bn|nn]/st per

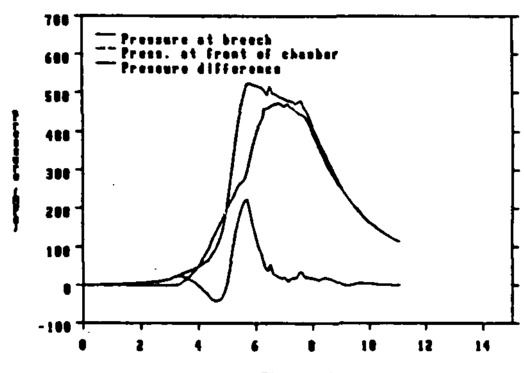

(g,s)/[bn|nn]/wk imp

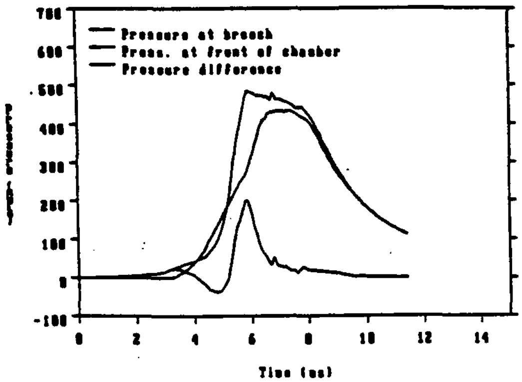

(g,s)/[bn|nn]/wk per

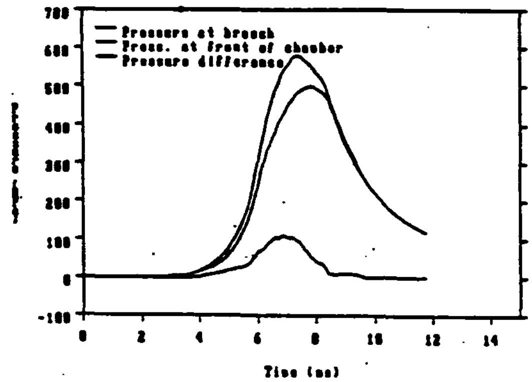

(g,s)/[nn|bn]/no no

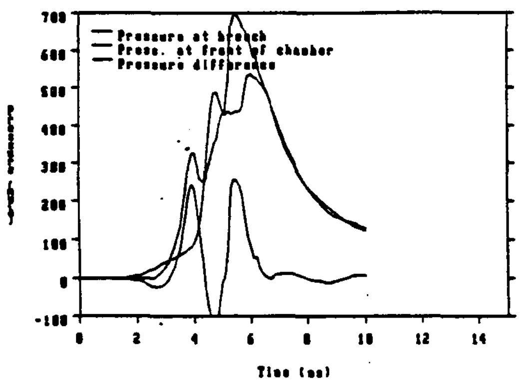

(g,s)/[nn|bn]/st imp

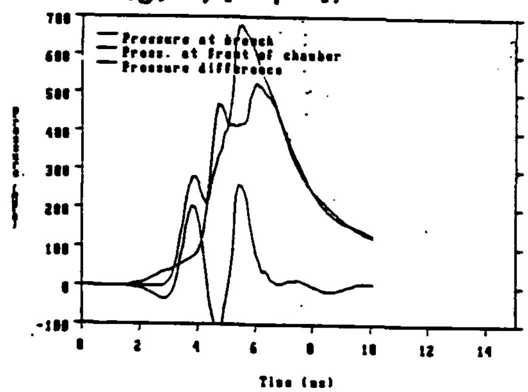

(g,s)/[nn|bn]/st per

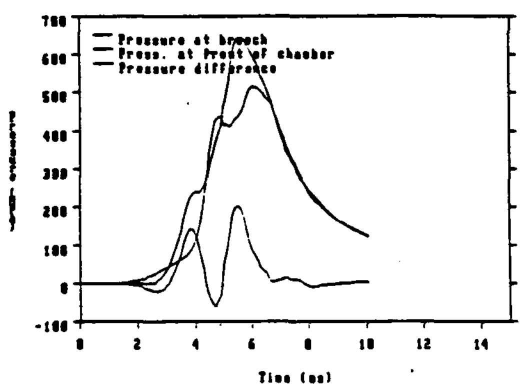

(g,s)/[nn|bn]/wk imp

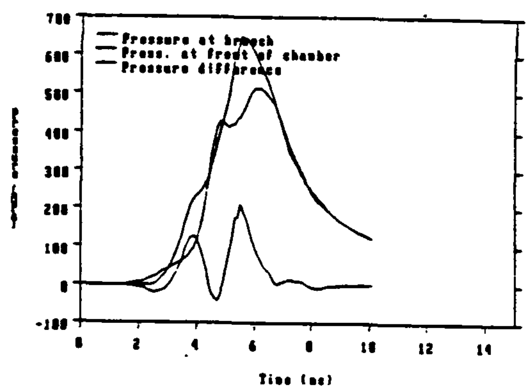

(g,s)/[nn|bn]/wk per

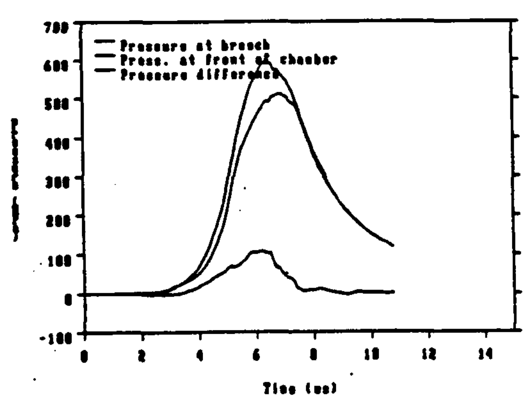

(g,s)/[nb|bn]/no no

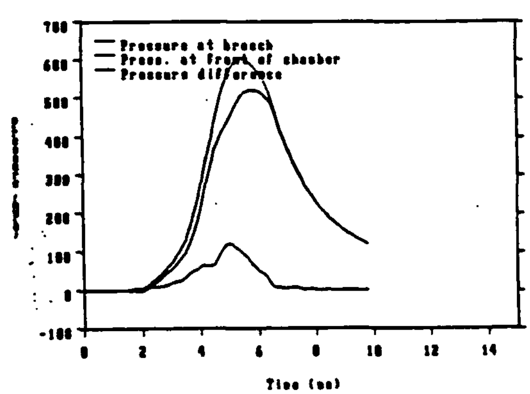

(g,s)/[nb|bn]/st imp

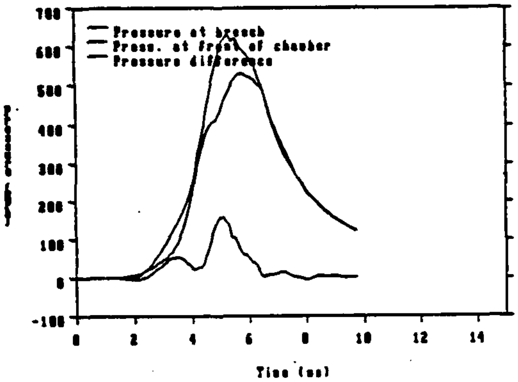

(g,s)/[nb|bn]/st per

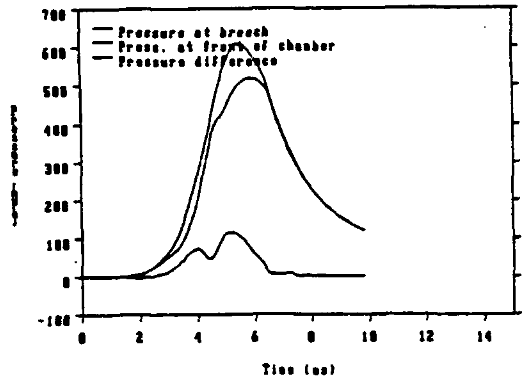

(g,s)/[nb|bn]/wk imp

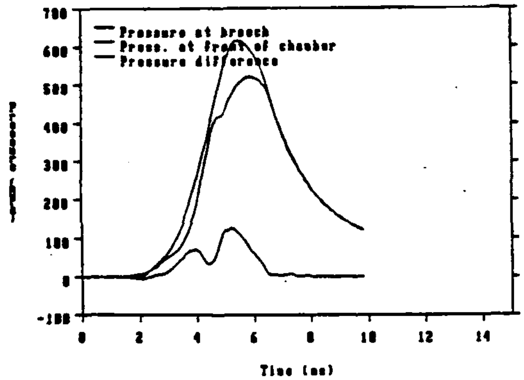

(g,s)/[nb|bn]/wk per

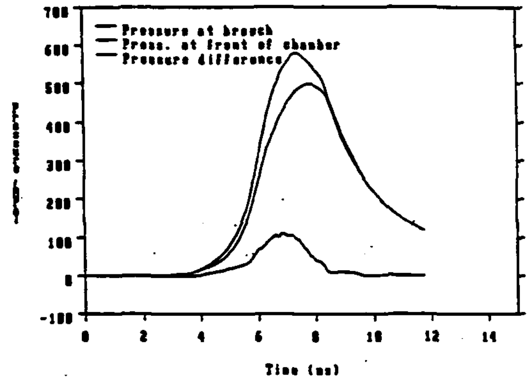

(g,s)/[nb|nn]/no no

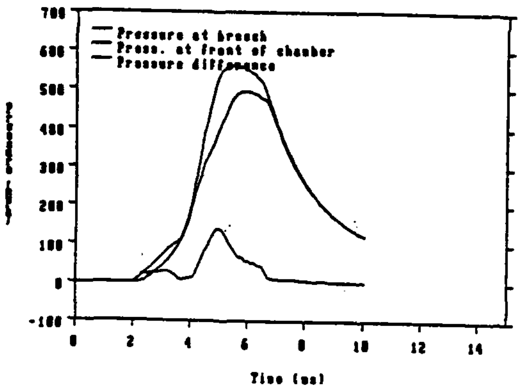

(g,s)/[nb|nn]/st imp

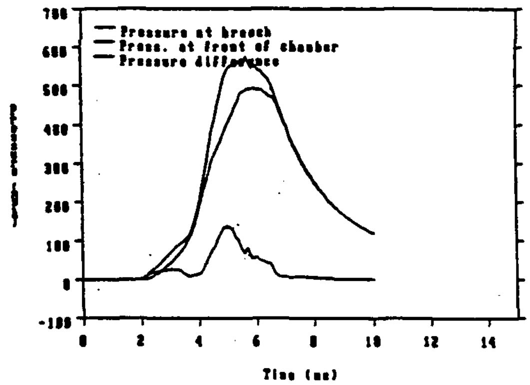

(g,s)/[nb|nn]/st per

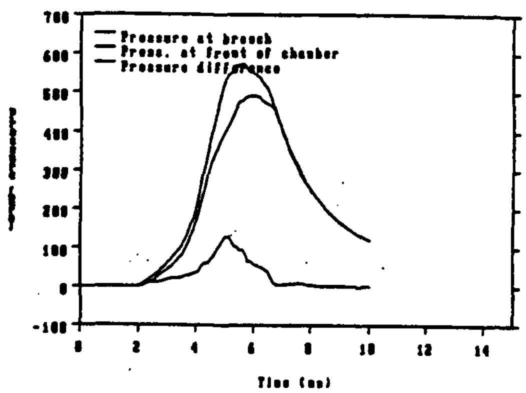

(g,s)/[nb|nn]/wk imp

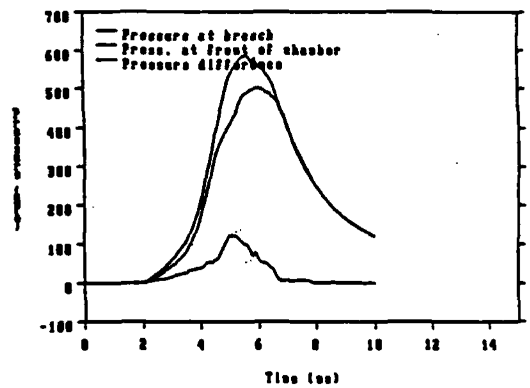

(g,s)/[nb|nn]/wk per

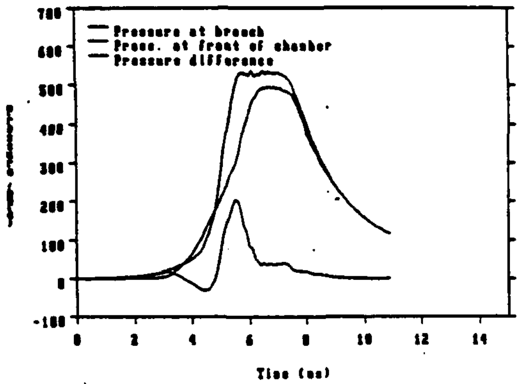

{g,s}/[bb|nn]/no no

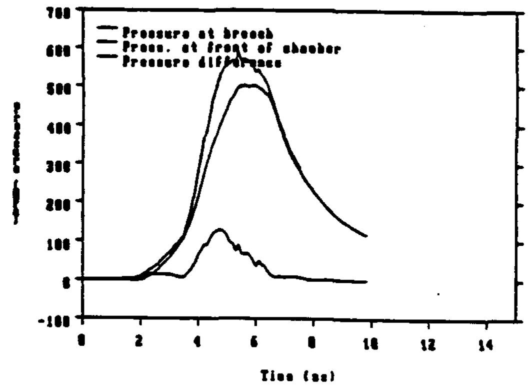

{g,s}/[bb|nn]/st imp

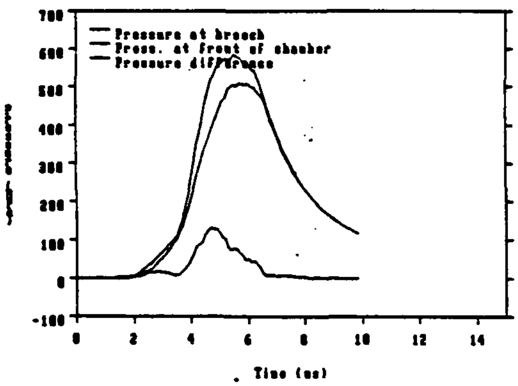

{g,s}/[bb|nn]/st per

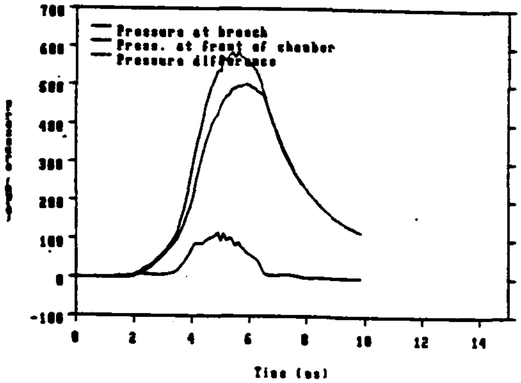

{g,s}/[bb|nn]/wk imp

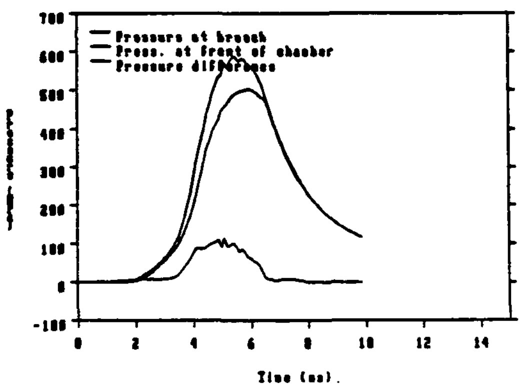

{g,s}/[bb|nn]/wk per

INTENTIONALLY LEFT BLANK.

APPENDIX E

Plots of Pressure-Time Traces for the Charge Configuration (g,g)

See Table 1 and APPENDIX B for the representations of the symbols used.

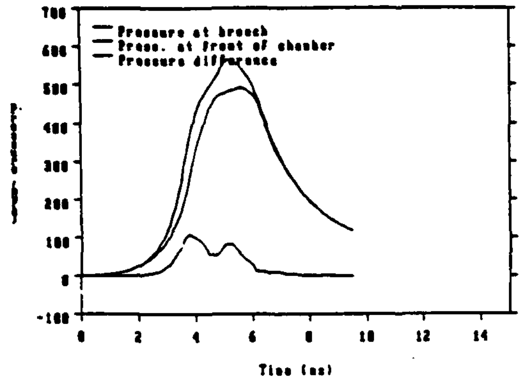

(g,g)/[uu|uu]/no no

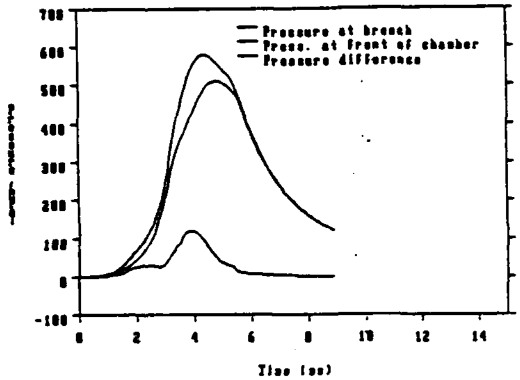

(g,g)/[uu|uu]/st imp

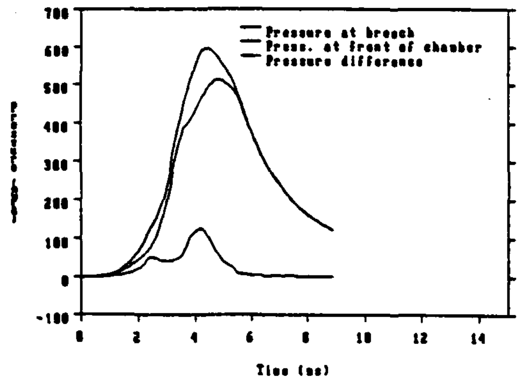

(g,s)/[uu|uu]/st per

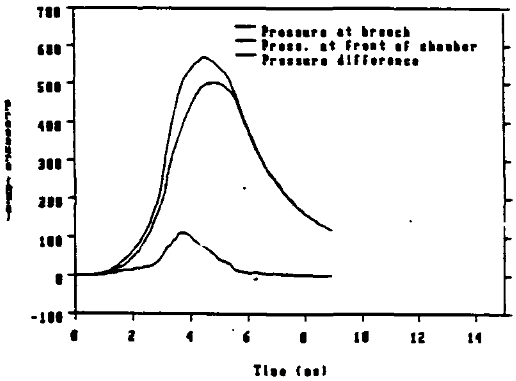

(g,g)/[uu|uu]/wk imp

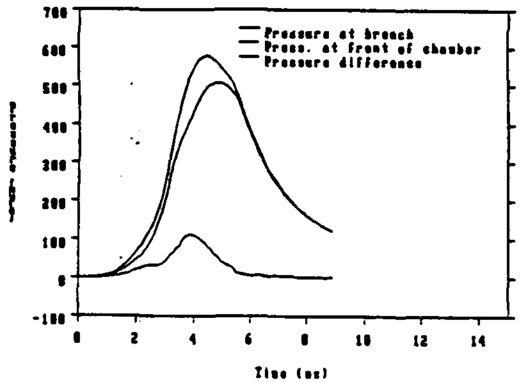

(g,g)/[uu|uu]/wk per

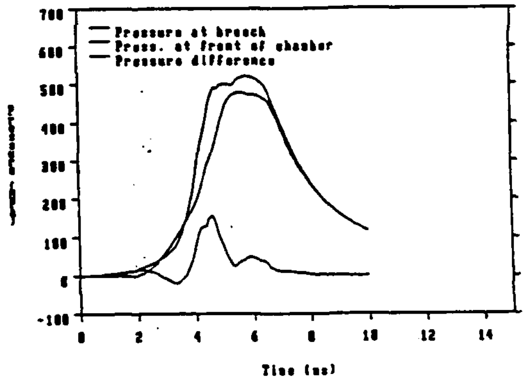

(g,g)/[uu|nn]/no no

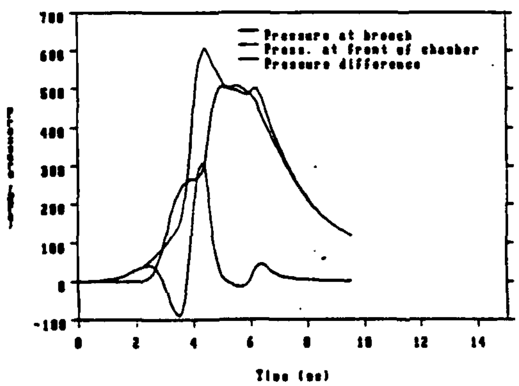

(g,g)/[uu|nn]/st imp

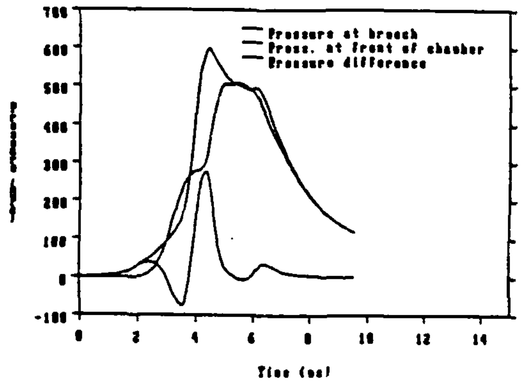

(g,g)/[uu|nn)/st per

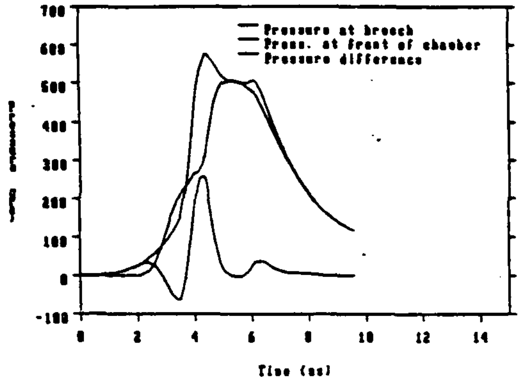

(g,g)/[uu|nn]/wk imp

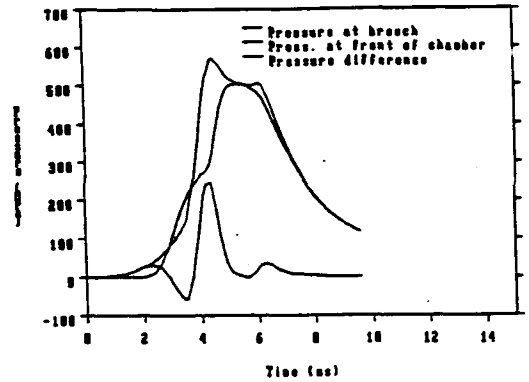

(g,g)/[uu|nn]/wk per

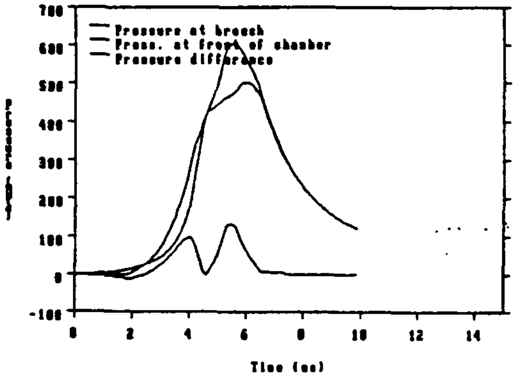

(g,g)/[nn|uu]/no no

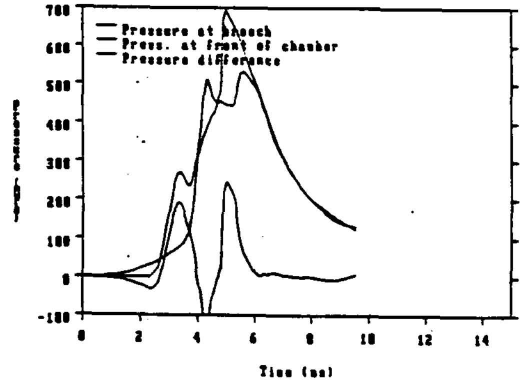

(g,g)/[nn|uu]/st imp

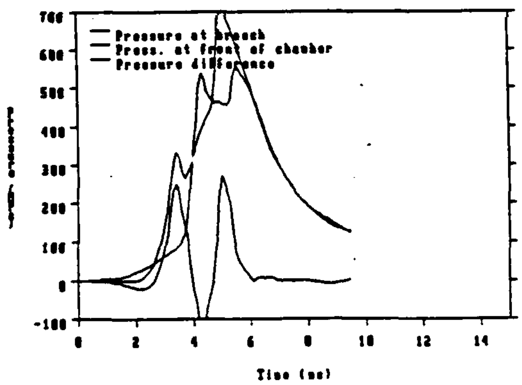

(g,g)/[nn|uu]/st per

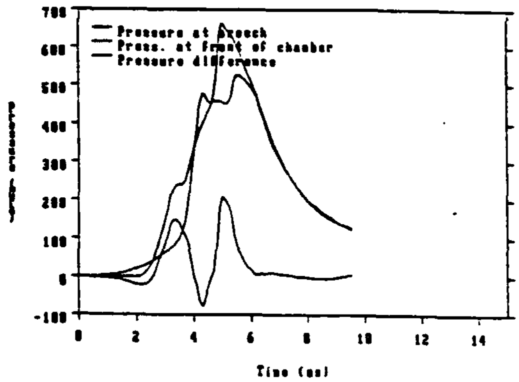

(g,g)/[nn|uu]/wk imp

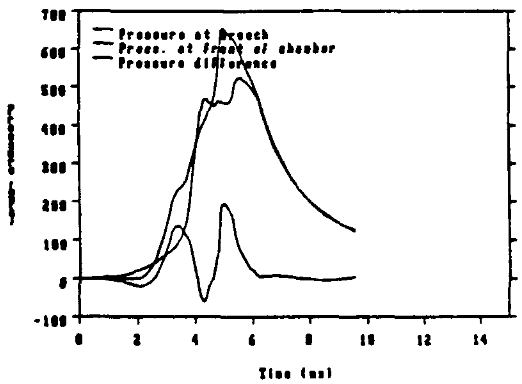

(g,g)/[nn|uu]/wk per

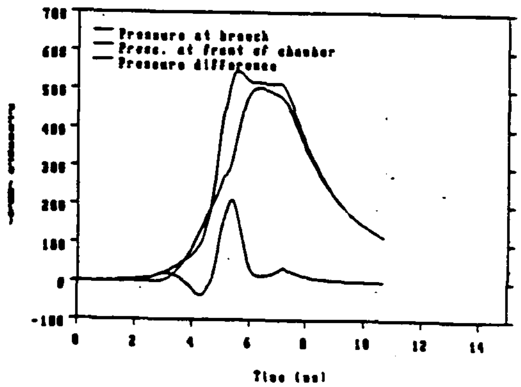

(g,g)/[bn|bn]/no no

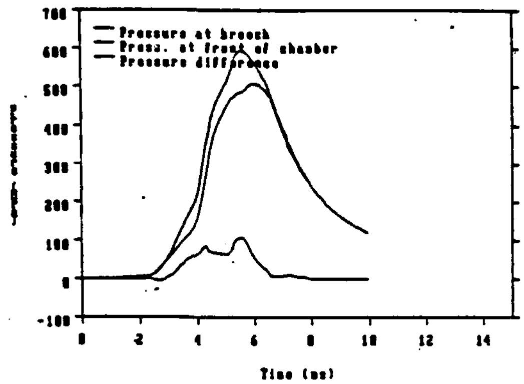

{g,g}/[bn|bn]/st imp

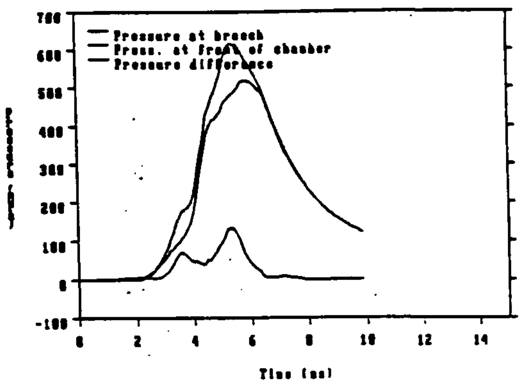

{g,g}/[bn|bn]/st per

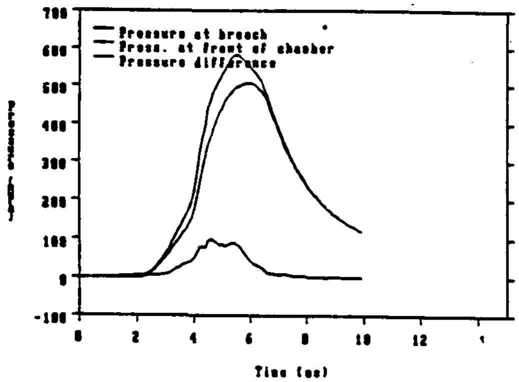

{g,g}/[bn|bn]/wk imp

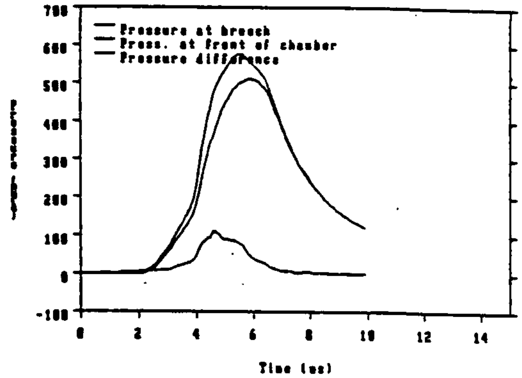

{g,g}/[bn|bn]/wk per

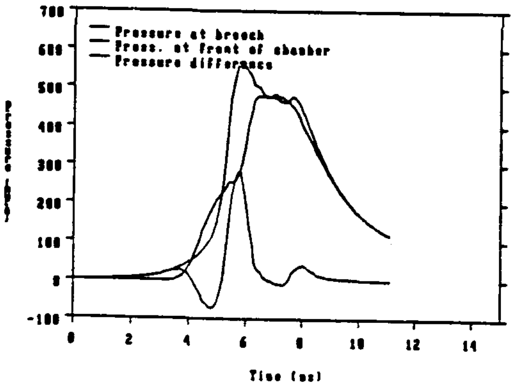

{g,g}/[bn|nn]/no no

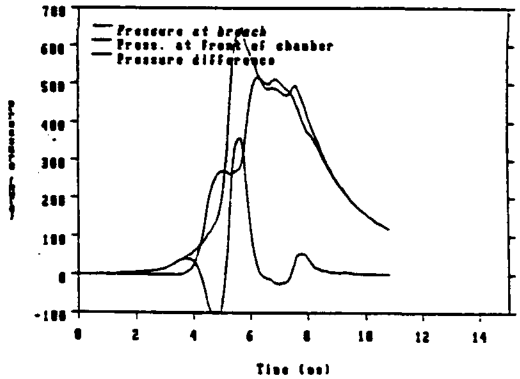

{g,g}/[bn|nn]/st imp

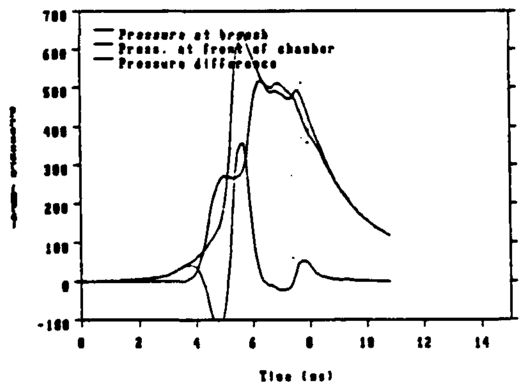

{g,g}/[bn|nn]/st per

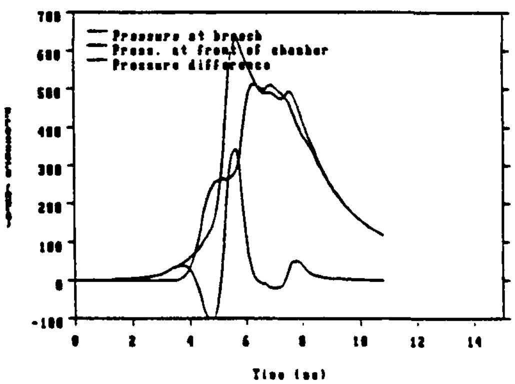

{g,g}/[bn|nn]/wk imp

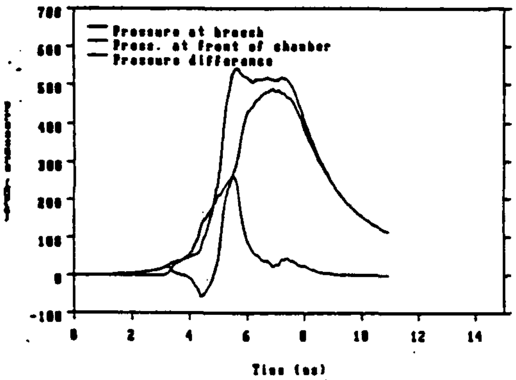

(g,g)/[bn|nn]/wk per

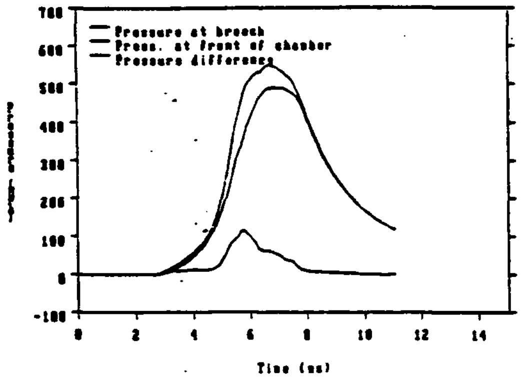

(g,g)/[nn|bn]/no no

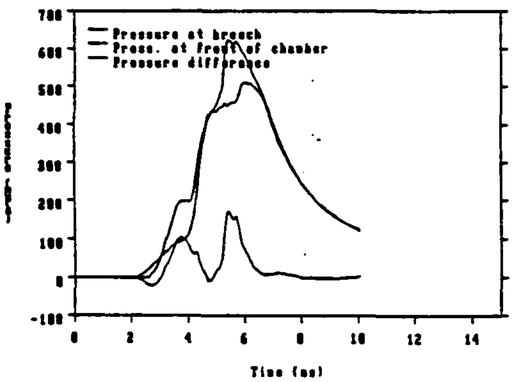

(g,g)/[nn|bn]/st imp

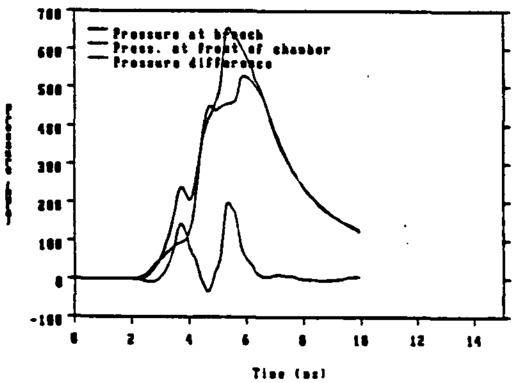

(g,g)/[nn|bn]/st per

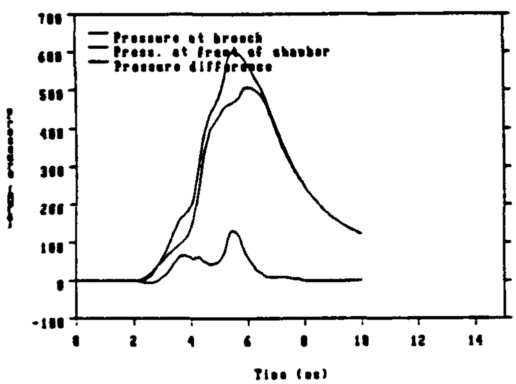

(g,g)/[nn|bn]/wk imp

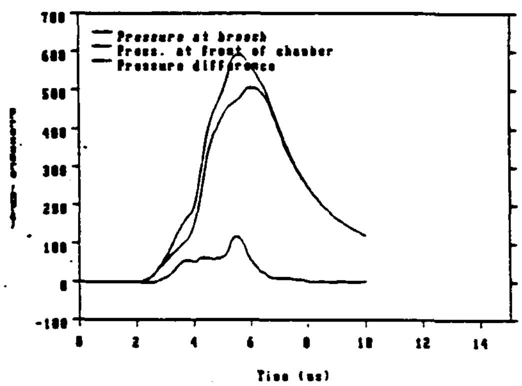

(g,g)/[nn|bn]/wk per

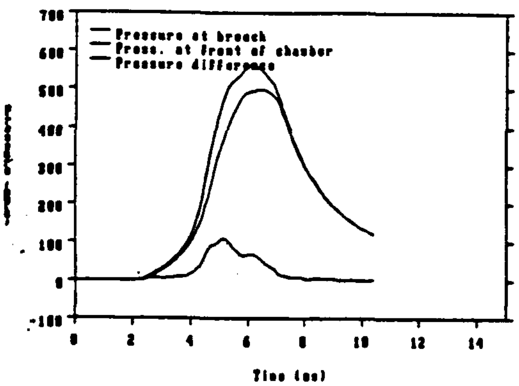

(g,g)/[nb|bn]/no no

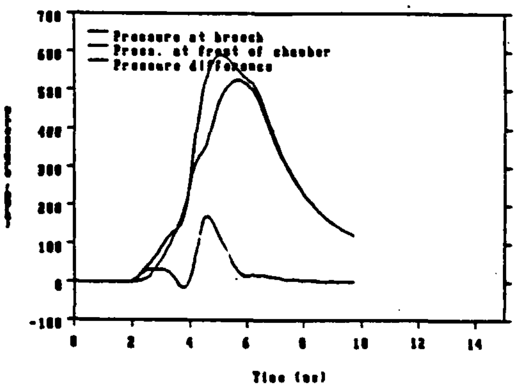

(g,g)/[nb|bn]/st imp

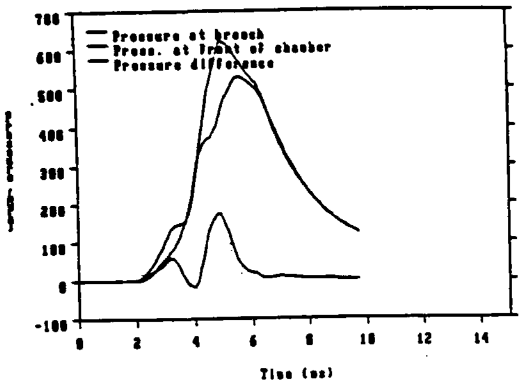

(g,g)/[nb|bn]/st per

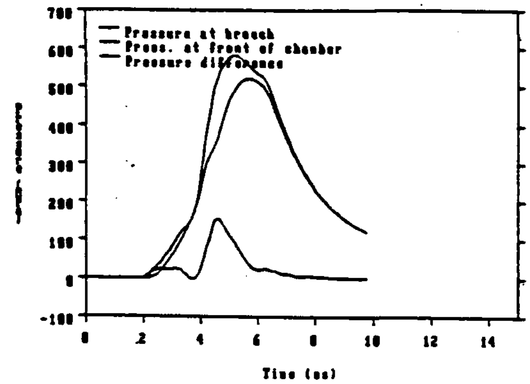

(g,g)/[nb|bn]/wk imp

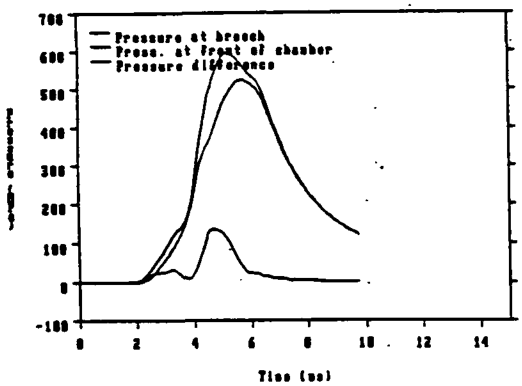

(g,g)/[nb|bn]/wk per

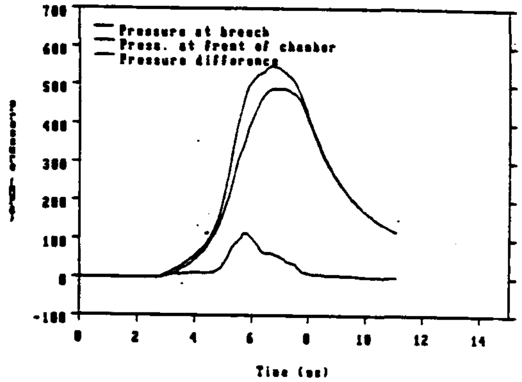

(g,g)/[nb|nn]/no no

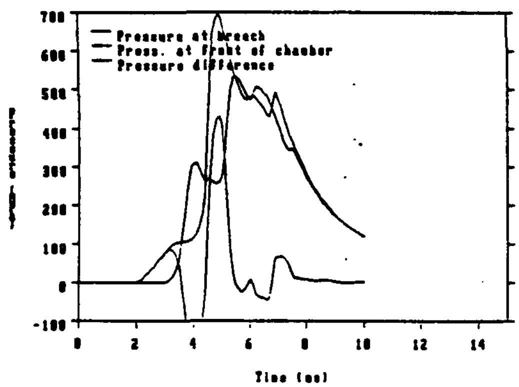

(g,g)/[nb|nn]/st imp

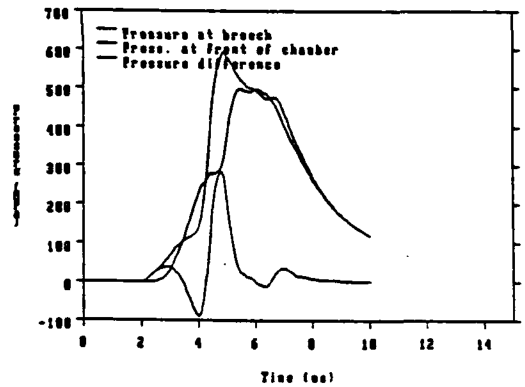

(g,g)/[nb|nn]/st per

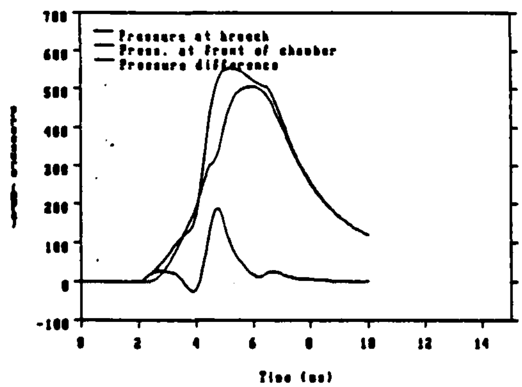

(g,g)/[nb|nn]/wk imp

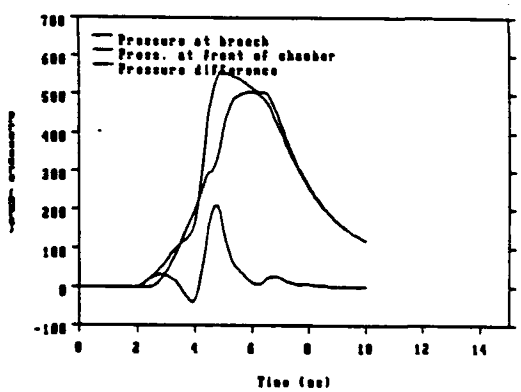

(g,g)/[nb|nn]/wk per

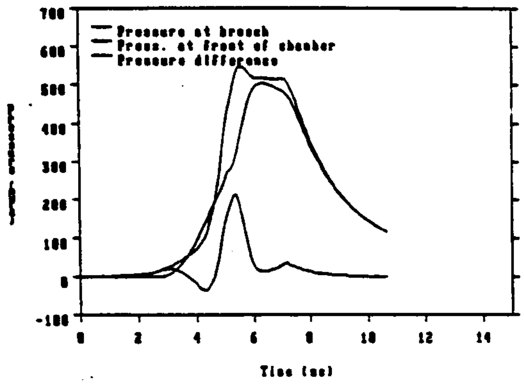

(g,g)/[bb|nn]/no no

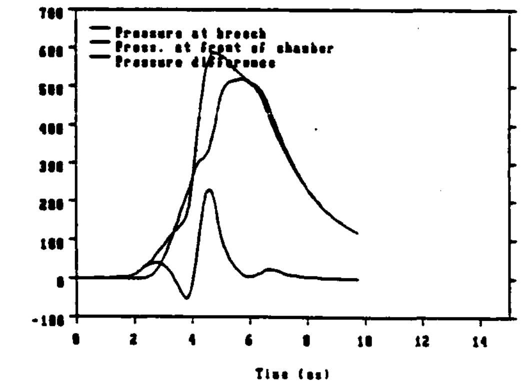

(g,g)/[bb|nn]/st imp

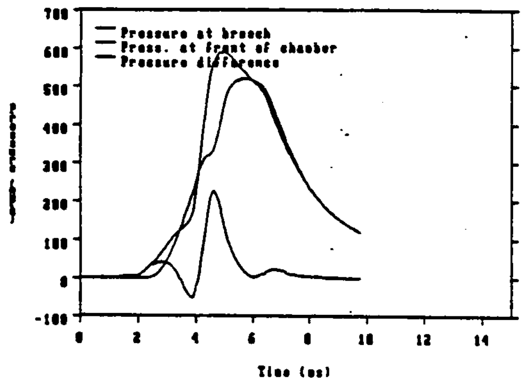

(g,g)/[bb|nn]/st per

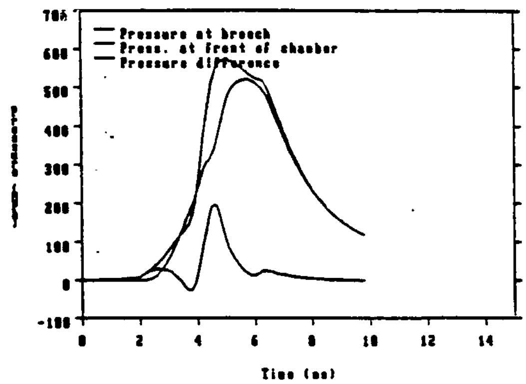

(g,g)/[bb|nn]/wk imp

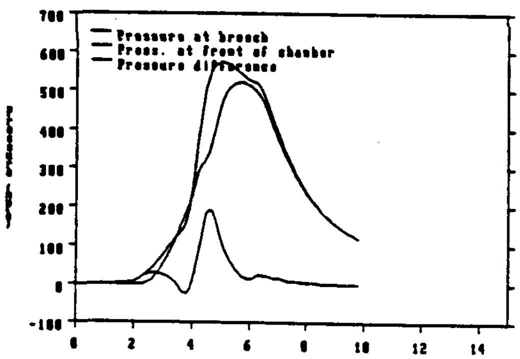

(g,g)/[bb|nn]/wk per

INTENTIONALLY LEFT BLANK.

No. of Copies	Organization
2	Administrator Defense Technical Info Center ATTN: DTIC-DDA Cameron Station Alexandria, VA 22304-6145
1	Commander U.S. Army Materiel Command ATTN: AMCAM 5001 Eisenhower Ave. Alexandria, VA 22333-0001
1	Commander U.S. Army Laboratory Command ATTN: AMSLC-DL 2800 Powder Mill Rd. Adelphi, MD 20783-1145
2	Commander U.S. Army Armament Research, Development, and Engineering Center ATTN: SMCAR-IMI-I Picatinny Arsenal, NJ 07806-5000
2	Commander U.S. Army Armament Research, Development, and Engineering Center ATTN: SMCAR-TDC Picatinny Arsenal, NJ 07806-5000
1	Director Benet Weapons Laboratory U.S. Army Armament Research, Development, and Engineering Center ATTN: SMCAR-CCB-TL Watervliet, NY 12189-4050
(Unclass. only) 1	Commander U.S. Army Rock Island Arsenal ATTN: SMCRI-TL/Technical Library Rock Island, IL 61299-5000
1	Director U.S. Army Aviation Research and Technology Activity ATTN: SAVRT-R (Library) M/S 219-3 Ames Research Center Moffett Field, CA 94035-1000
1	Commander U.S. Army Missile Command ATTN: AMSMI-RD-CS-R (DOC) Redstone Arsenal, AL 35898-5010

No. of Copies	Organization
1	Commander U.S. Army Tank-Automotive Command ATTN: ASQNC-TAC-DIT (Technical Information Center) Warren, MI 48397-5000
1	Director U.S. Army TRADOC Analysis Command ATTN: ATRC-WSR White Sands Missile Range, NM 88002-5502
1	Commandant U.S. Army Field Artillery School ATTN: ATSF-CSI Ft. Sill, OK 73503-5000
(Class. only) 1	Commandant U.S. Army Infantry School ATTN: ATSH-CD (Security Mgr.) Fort Benning, GA 31905-5660
(Unclass. only) 1	Commandant U.S. Army Infantry School ATTN: ATSH-CD-CSO-OR Fort Benning, GA 31905-5660
1	WL/MNOI Eglin AFB, FL 32542-5000
	Aberdeen Proving Ground
2	Dir, USAMSAA ATTN: AMXSY-D AMXSY-MP, H. Cohen
1	Cdr, USATECOM ATTN: AMSTE-TC
3	Cdr, CRDEC, AMCCOM ATTN: SMCCR-RSP-A SMCCR-MU SMCCR-MSI
1	Dir, VLAMO ATTN: AMSLC-VL-D
10	Dir, USABRL ATTN: SLCBR-DD-T

No. of Copies	Organization
1	Commander U.S. Army Concepts Analysis Agency ATTN: D. Hardison 8120 Woodmont Ave. Bethesda, MD 20014
1	C.I.A. 01R/DB/Standard Washington, DC 20505
1	Director U.S. Army Ballistic Missile Defense Systems Command Advanced Technology Center P. O. Box 1500 Huntsville, AL 35807-3801
1	Chairman DOD Explosives Safety Board Room 856-C Hoffman Bldg. 1 2461 Eisenhower Ave. Alexandria, VA 22331-0600
1	Department of the Army Office of the Product Manager 155mm Howitzer, M109A6, Paladin ATTN: SFAE-AR-HIP-IP, Mr. R. De Kleine Picatinny Arsenal, NJ 07806-5000
2	Commander Production Base Modernization Agency U.S. Army Armament Research, Development, and Engineering Center ATTN: AMSMC-PBM, A. Siklosi AMSMC-PBM-E, L. Laibson Picatinny Arsenal, NJ 07806-5000
3	PEO-Armaments Project Manager Tank Main Armament Systems ATTN: AMCPM-TMA/K. Russell AMCPM-TMA-105 AMCPM-TMA-120, C. Roller Picatinny Arsenal, NJ 07806-5000

No. of Copies	Organization
15	Commander U.S. Army Armament Research, Development, and Engineering Center ATTN: SMCAR-AEE SMCAR-AEE-B, A. Beardell D. Downs S. Einstein S. Westley S. Bernstein J. Rutkowski B. Brodman R. Cirincione A. Grabowsky P. Hui J. O'Reilly P. O'Reilly N. DeVries SMCAR-AES, S. Kaplowitz, Bldg. 321 Picatinny Arsenal, NJ 07806-5000
2	Commander U.S. Army Armament Research, Development, and Engineering Center ATTN: SMCAR-CCD, D. Spring SMCAR-CCH-V, C. Mandala Picatinny Arsenal, NJ 07806-5000
1	Commander U.S. Army Armament Research, Development, and Engineering Center ATTN: SMCAR-HFM, E. Barrieres Picatinny Arsenal, NJ 07806-5000
1	Commander U.S. Army Armament Research, Development, and Engineering Center ATTN: SMCAR-FSA-T, M. Salsbury Picatinny Arsenal, NJ 07806-5000
1	Commander, USACECOM R&D Technical Library ATTN: ASQNC-ELC-IS-L-R, Myer Center Fort Monmouth, NJ 07703-5301

No. of Copies	Organization
1	Commander U.S. Army Harry Diamond Laboratories ATTN: SLCHD-TA-L 2800 Powder Mill Rd. Adelphi, MD 20783-1145
1	Commandant U.S. Army Aviation School ATTN: Aviation Agency Fort Rucker, AL 36360
2	Program Manager U.S. Army Tank-Automotive Command ATTN: AMCPM-ABMS, T. Dean (2 cps) Warren, MI 48092-2498
1	Program Manager U.S. Army Tank-Automotive Command Fighting Vehicles Systems ATTN: SFAE-ASM-BV Warren, MI 48092-2498
1	Project Manager Abrams Tank System ATTN: SFAE-ASM-AB Warren, MI 48397-5000
1	Director HQ, TRAC RPD ATTN: ATCD-MA Fort Monroe, VA 23651-5143
2	Director U.S. Army Materials Technology Laboratory ATTN: SLCMT-ATL (2 cps) Watertown, MA 02172-0001
1	Commander U.S. Army Research Office ATTN: Technical Library P.O. Box 12211 Research Triangle Park, NC 27709-2211
1	Commander U.S. Army Belvoir Research and Development Center ATTN: STRBE-WC Fort Belvoir, VA 22060-5006

No. of Copies	Organization
1	Director U.S. Army TRAC-Ft. Lee ATTN: ATRC-L, Mr. Cameron Fort Lee, VA 23801-6140
1	Commandant U.S. Army Command and General Staff College Fort Leavenworth, KS 66027
1	Commandant U.S. Army Special Warfare School ATTN: Rev and Trng Lit Div Fort Bragg, NC 28307
3	Commander Radford Army Ammunition Plant ATTN: SMCAR-QA/HI LIB (3 cps) Radford, VA 24141-0298
1	Commander U.S. Army Foreign Science and Technology Center ATTN: AMXST-MC-3 220 Seventh Street, NE Charlottesville, VA 22901-5396
2	Commander Naval Sea Systems Command ATTN: SEA 62R SEA 64 Washington, DC 20362-5101
1	Commander Naval Air Systems Command ATTN: AIR-954-Technical Library Washington, DC 20360
1	Naval Research Laboratory Technical Library Washington, DC 20375
2	Commandant U.S. Army Field Artillery Center and School ATTN: ATSF-CO-MW, E. Dublisky (2 cps) Fort Sill, OK 73503-5600

No. of Copies	Organization
1	Office of Naval Research ATTN: Code 473, R. S. Miller 800 N. Quincy Street Arlington, VA 22217-9999
3	Commandant U.S. Army Armor School ATTN: ATZK-CD-MS, M. Falkovitch (3 cps) Armor Agency Fort Knox, KY 40121-5215
2	Commander U.S. Naval Surface Warfare Center ATTN: J. P. Consaga C. Gotzmer Indian Head, MD 20640-5000
4	Commander Naval Surface Warfare Center ATTN: Code 240, S. Jacobs Code 730 Code R-13, K. Kim R. Bernecker Silver Spring, MD 20903-5000
2	Commanding Officer Naval Underwater Systems Center ATTN: Code 5B331, R. S. Lazar Technical Library Newport, RI 02840
1	Director Benet Weapons Laboratories ATTN: SMCAR-CCB-RA, G. P. O'Hara Watervliet, NY 12189-4050
4	Commander Dahlgren Division Naval Surface Warfare Center ATTN: Code G30, Guns and Munitions Division Code G301, D. Wilson Code G32, Gun Systems Branch Code E23, Technical Library Dahlgren, VA 22448-5000

No. of Copies	Organization
3	Commander Naval Weapons Center ATTN: Code 388, C. F. Price Code 3895, T. Parr Information Science Division China Lake, CA 93555-6001
1	OSD/SDIO/IST ATTN: Dr. Len Caveny Pentagon Washington, DC 20301-7100
3	Commander Naval Ordnance Station ATTN: T. C. Smith D. Brooks Technical Library Indian Head, MD 20640-5000
1	OLAC PL/TSTL ATTN: D. Shiplett Edwards AFB, CA 93523-5000
1	AFATL/DLYV Eglin AFB, FL 32542-5000
1	AFATL/DLXP Eglin AFB, FL 32542-5000
1	AFATL/DLJE Eglin AFB, FL 32542-5000
1	AFELM, The Rand Corporation ATTN: Library D 1700 Main Street Santa Monica, CA 90401-3297
3	AAI Corporation ATTN: J. Hebert J. Frankle D. Cleveland P.O. Box 126 Hunt Valley, MD 21030-0126
2	Aerojet Solid Propulsion Company ATTN: P. Micheli L. Torreyson Sacramento, CA 96813

No. of Copies	Organization
3	AL/LSCF ATTN: J. Levine L. Quinn T. Edwards Edwards AFB, CA 93523-5000
1	AVCO Everett Research Laboratory ATTN: D. Stickler 2385 Revere Beach Parkway Everett, MA 02149-5936
1	General Electric Company Tactical Systems Department ATTN: J. Mandzy 100 Plastics Ave. Pittsfield, MA 01201-3698
1	IITRI ATTN: M. J. Klein 10 W. 35th Street Chicago, IL 60616-3799
1	Hercules, Inc. Allegheny Ballistics Laboratory ATTN: William B. Walkup P.O. Box 210 Rocket Center, WV 26726
1	Hercules, Inc. Radford Army Ammunition Plant ATTN: E. Hibshman Radford, VA 24141-0299
1	Hercules, Inc. Hercules Plaza ATTN: B. M. Riggleman Wilmington, DE 19894
3	Director Lawrence Livermore National Laboratory ATTN: L-355, A. Buckingham M. Finger L-324, M. Constantino P.O. Box 808 Livermore, CA 94550-0622

No. of Copies	Organization
1	Olin Corporation Badger Army Ammunition Plant ATTN: F. E. Wolf Baraboo, WI 53913
3	Olin Ordnance ATTN: E. J. Kirschke A. F. Gonzalez D. W. Worthington P.O. Box 222 St. Marks, FL 32355-0222
1	Olin Ordnance ATTN: H. A. McElroy 10101 9th Street, North St. Petersburg, FL 33716
1	Paul Gough Associates, Inc. ATTN: Dr. Paul S. Gough 1048 South Street Portsmouth, NH 03801-5423
1	Physics International Company ATTN: Library, H. Wayne Wampler 2700 Merced Street San Leandro, CA 98457-5602
1	Princeton Combustion Research Laboratory, Inc. ATTN: M. Summerfield 475 U.S. Highway One Monmouth Junction, NJ 08852-9650
2	Rockwell International Rocketdyne Division ATTN: BA08, J.E. Flanagan J. Gray 6633 Canoga Ave. Canoga Park, CA 91303-2703
1	Thiokol Corporation Huntsville Division ATTN: Technical Library Huntsville, AL 35807

No. of Copies	Organization
1	Sverdrup Technology, Inc. ATTN: Dr. John Deur 2001 Aerospace Parkway Brook Park, OH 44142
2	Thiokol Corporation Elkton Division ATTN: R. Biddle Technical Library P.O. Box 241 Elkton, MD 21921-0241
1	Veritay Technology, Inc. ATTN: E. Fisher 4845 Millersport Highway East Amherst, NY 14501-0305
1	Universal Propulsion Company ATTN: H. J. McSpadden 25401 North Central Ave. Phoenix, AZ 85027-7837
1	Battelle ATTN: TACTEC Library, J.N. Huggins 505 King Ave. Columbus, OH 43201-2693
1	Brigham Young University Department of Chemical Engineering ATTN: M. Beckstead Provo, UT 84601
1	California Institute of Technology 204 Karman Laboratory Main Stop 301-46 ATTN: F.E.C. Culick 1201 E. California Street Pasadena, CA 91109
1	California Institute of Technology Jet Propulsion Laboratory ATTN: L. D. Strand, MS 512/102 4800 Oak Grove Drive Pasadena, CA 91109-8099

No. of Copies	Organization
1	University of Illinois Department of Mechanical/Industrial Engineering ATTN: H. Krier 144 MEB; 1206 N. Green Street Urbana, IL 61801-2978
1	University of Massachusetts Department of Mechanical Engineering ATTN: K. Jakus Amherst, MA 01002-0014
1	University of Minnesota Department of Mechanical Engineering ATTN: E. Fletcher Minneapolis, MN 55414-3368
3	Georgia Institute of Technology School of Aerospace Engineering ATTN: B.T. Zim E. Price W.C. Strahle Atlanta, GA 30332
1	Institute of Gas Technology ATTN: D. Gidaspow 3424 S. State Street Chicago, IL 60616-3896
1	Johns Hopkins University Applied Physics Laboratory Chemical Propulsion Information Agency ATTN: T. Christian Johns Hopkins Road Laurel, MD 20707-0690
1	Massachusetts Institute of Technology Department of Mechanical Engineering ATTN: T. Toong 77 Massachusetts Ave. Cambridge, MA 02139-4307
1	Pennsylvania State University Department of Mechanical Engineering ATTN: V. Yang University Park, PA 16802-7501

No. of Copies	Organization
1	Pennsylvania State University Department of Mechanical Engineering ATTN: K. Kuo University Park, PA 16802-7501
1	Pennsylvania State University Assistant Professor Department of Mechanical Engineering ATTN: Dr. Stefan T. Thynell 219 Hallowell Building University Park, PA 16802-7501
1	Pennsylvania State University Director, Gas Dynamics Laboratory Department of Mechanical Engineering ATTN: Dr. Gary S. Settles 303 Mechanical Engineering Building University Park, PA 16802-7501
1	SRI International Propulsion Sciences Division ATTN: Technical Library 333 Ravenwood Ave. Menlo Park, CA 94025-3493
1	Rensselaer Ploytechnic Institute Department of Mathematics Troy, NY 12181
2	Director Los Alamos Scientific Laboratory ATTN: T3, D. Butler M. Division, B. Craig P.O. Box 1663 Los Alamos, NM 87544
1	General Applied Sciences Laboratory ATTN: J. Erdos 77 Raynor Ave. Ronkonkama, NY 11779-6649
1	Battelle PNL ATTN: Mr. Mark Garnich P.O. Box 999 Richland, WA 99352

No. of Copies	Organization
1	Stevens Institute of Technology Davidson Laboratory ATTN: R. McAlevy III Castle Point Station Hoboken, NJ 07030-5907
1	Rutgers University Department of Mechanical and Aerospace Engineering ATTN: S. Temkin University Heights Campus New Brunswick, NJ 08903
1	University of Southern California Mechanical Engineering Department ATTN: 0HE200, M. Gerstein Los Angeles, CA 90089-5199
1	University of Utah Department of Chemical Engineering ATTN: A. Baer Salt Lake City, UT 84112-1194
1	Washington State University Department of Mechanical Engineering ATTN: C. T. Crowe Pullman, WA 99163-5201
1	Alliant Techsystems, Inc. ATTN: R. E. Tompkins MN38-3300 5700 Smetana Drive Minnetonka, MN 55343
1	Alliant Techsystems, Inc. ATTN: J. Kennedy 7225 Northland Drive Brooklyn Park, MN 55428
1	Science Applications, Inc. ATTN: R. B. Edelman 23146 Cumorah Crest Drive Woodland Hills, CA 91364-3710
1	Battelle Columbus Laboratories ATTN: Mr. Victor Levin 505 King Ave. Columbus, OH 43201-2693

No. of Copies	Organization
1	Allegheny Ballistics Laboratory Propulsion Technology Department Hercules Aerospace Company ATTN: Mr. Thomas F. Farabaugh P.O. Box 210 Rocket Center, WV 26726
1	MBR Research Inc. ATTN: Dr. Moshe Ben-Reuven 601 Ewing St., Suite C-22 Princeton, NJ 08540
	Aberdeen Proving Ground
1	Cdr, CSTA ATTN: STECS-PO, R. Hendricksen

USER EVALUATION SHEET/CHANGE OF ADDRESS

This laboratory undertakes a continuing effort to improve the quality of the reports it publishes. Your comments/answers below will aid us in our efforts.

1. Does this report satisfy a need? (Comment on purpose, related project, or other area of interest for which the report will be used.) ______________________________

2. How, specifically, is the report being used? (Information source, design data, procedure, source of ideas, etc.) ______________________________

3. Has the information in this report led to any quantitative savings as far as man-hours or dollars saved, operating costs avoided, or efficiencies achieved, etc? If so, please elaborate. ______________________________

4. General Comments. What do you think should be changed to improve future reports? (Indicate changes to organization, technical content, format, etc.) ______________________________

BRL Report Number BRL-TR-3373 Division Symbol ______________

Check here if desire to be removed from distribution list. ____

Check here for address change. ____

Current address: Organization ______________
Address ______________

DEPARTMENT OF THE ARMY
Director
U.S. Army Ballistic Research Laboratory
ATTN: SLCBR-DD-T
Aberdeen Proving Ground, MD 21005-5066

OFFICIAL BUSINESS

BUSINESS REPLY MAIL
FIRST CLASS PERMIT No 0001, APG, MD

Postage will be paid by addressee.

NO POSTAGE NECESSARY IF MAILED IN THE UNITED STATES

Director
U.S. Army Ballistic Research Laboratory
ATTN: SLCBR-DD-T
Aberdeen Proving Ground, MD 21005-5066